Rheology
Phytoplankton
Organic aggregates
Surface microlayer
Dissolved organic matter (DOM)

Rhéologie
Phytoplancton
Agrégats organiques
Microcouche superficielle
Matière organique dissoute

Bulk-phase viscoelastic properties of seawater

Ian R. JENKINSON *

Université de Nice-Sophia-Antipolis, Laboratoire de Biologie et d'Écologie marines, 06108 Nice Cedex 02, France; and Alfred-Wegener-Institut für Polar- und Meeresforschung, 27515 Bremerhaven, Germany.

* *Address for correspondence:* Agence de Conseil et de Recherche Océanographiques, Lavergne, 19320 La Roche-Canillac, France.

Received 24/07/92, in revised form 30/05/93, accepted 7/06/93.

ABSTRACT

Deformation and mixing in any medium are controlled by its viscosity and elasticity. The present study provides preliminary information, at oceanic shear rates, on the viscosity and elasticity in the bulk phase of seawater.

Thirty-two samples of seawater, obtained on cruises at four times of year in a meso-oligotrophic part of the Mediterranean, were measured for bulk-phase viscoelastic properties in an oscillating-shear Couette flow with measuring gap 0.5 mm, over shear rates $\dot{\gamma}$ from 0.0021 to 0.286 s^{-1}. Fifteen samples were obtained on a single cruise in the German Bight, North Sea, when *Phaeocystis* blooms were taking place, and these were similarly measured at $\dot{\gamma}$ from 0.0021 to 0.973 s^{-1}.

The bulk-phase measurements suffered interference contributed by the surface film. The interference mechanism was investigated, and a method was developed to correct for it, which permitted extraction of the bulk-phase viscosity. While extraction of bulk-phase elastic effects was possible only in the most thickened Mediterranean samples, in the generally thicker North Sea samples bulk-phase elasticity was closely related to bulk-phase excess (polymeric) viscosity.

At $\dot{\gamma} = 0.0021$ s^{-1}, viscosity, η, in the Mediterranean samples ranged from 0.17 to 19 (mean 3.5, n = 23) times the average solution viscosity, $\overline{\eta_w}$, which is $\dot{\gamma}$-independent and contributed principally by water and salt. Corresponding values for the German Bight samples were 0.99 to 127 (mean 52, n = 5) times $\overline{\eta_w}$.

For each cruise, the overall excess viscosity, $\eta_E = \eta - \eta_w$, showed a power-law relationship with $\dot{\gamma}$ such that $\eta_E = k.\dot{\gamma}^{-P}$. For the five different cruises, P varied from 1.1 to 1.5. Such high values of P indicate that thickening is contributed principally by cross-linked polymer gel rather than by overlapping chains. The elastic modulus G' was very variable, with sample maxima of 100 and 300 μPa in the Mediterranean and North Seas respectively.

Thickening (determined as both η_E and G') was heterogeneous, with a variability coefficient (SD/mean) from 1 to 3 for different cruises and values of $\dot{\gamma}$. In the three Mediterranean cruises in which duplicate measurements were made for the same samples, all the variability could be accounted for by in-sample variability, suggesting that centimetre-scale flocculation-type processes were responsible. Gaussian

Publication No. 643 from the Alfred-Wegener-Institut

standard deviation SD_G was constant (indicating self-similarity) for the higher values of η_E both the Mediterranean and North Sea studies a well as for G' in the North Sea study. At the lower end of the η_E and G' distributions, SD_G was higher, due to experimental variability. Over a range of appropriate shear rates, the turbulent (Kolmogorov) length scale L was calculated using the mean viscosities measured. The calculations suggest that, when turbulence is low or biological activity high, L is considerably higher than values previously supposed, and mixing correspondingly reduced. The heterogeneous nature of both η_E and G' must furthermore increase intermittence in both turbulence and mixing. It is concluded that a significant part of the sea functions as a lumpy, biopolymeric gel in which small-scale ($\leq$ 100.L) flow and mixing are under strong biological influence.

Oceanologica Acta, 1993. **16**, 4, 317-334.

RÉSUMÉ

Propriétés viscoélastiques de la phase volumique d'eau de mer

La déformation et le mélange de tout milieu sont contrôlés par sa viscosité et son élasticité. L'étude présente fournit des informations préliminaires, à des vitesses de déformation ambiantes en mer, sur la viscosité et l'élasticité en phase volumique (c'est-à-dire celle de masse) de l'eau de mer.

Trente-deux échantillons d'eau de mer ont été prélevés pendant quatre sorties réparties sur toute une année dans une zone méso-oligotrophe de la Méditerranée. Des mesures des propriétés viscoélastiques de la phase volumique ont été effectuées sur ces échantillons en régime d'écoulement oscillant entre deux cylindres coaxiaux, avec un entrefer de 0,5 mm et sur une gamme de vitesses de cisaillement $\dot{\gamma}$ entre 0,0021 et 0,286 s^{-1}. Quinze échantillons ont été prélevés également en baie d'Helgoland (Mer du Nord) durant des efflorescences de *Phaeocystis*, puis ils ont été mesurés de manière identique à des valeurs de $\dot{\gamma}$ entre 0,0021 et 0,973 s^{-1}.

Les mesures effectuées sur la phase en volume ont été parasitées par des effets amenés par la phase superficielle. Le mécanisme responsable de ces effets parasites a été étudié et une méthode pour en tenir compte a été développée. A cause de ces parasites les effets élastiques de la phase volumique n'ont pas pu être décelés dans la plupart des échantillons méditerranéens, mais dans l'eau de la Mer du Nord l'élasticité était étroitement liée à la viscosité excédentaire (due aux polymères).

Pour $\dot{\gamma}$ = 0,0021 s^{-1}, la viscosité, η, mesurée sur les échantillons de la Méditerranée, a varié entre 0,17 et 19 (moyenne 3,5; n = 23) fois la «viscosité du solvant», $\overline{\eta_w}$ qui est indépendante de $\dot{\gamma}$ et qui provient principalement de l'eau et du sel. Les valeurs correspondantes pour la baie d'Helgoland ont été 0,99 à 127 (moyen 52, n = 5) fois $\overline{\eta_w}$.

La viscosité excédentaire, $\eta_E = \eta - \eta_w$, obéit à une loi en puissance : $\eta_E = k.\ \dot{\gamma}^{-P}$. Pour chacune des cinq sorties en mer, la valeur globale de P s'est située entre 1,1 et 1,5. Ces valeurs importantes de P démontrent que l'épaississement est produit par des gels de polymères portant de nombreuses zones de jonction. Le module élastique G' a été très variable, avec un maximum de 100 ou de 300 µPa, respectivement pour l'étude en Méditerranée ou celle en Mer du Nord.

Ces épaississements (η_E et G') étaient hétérogènes, le coefficient de variabilité (écart-type/moyenne) étant de 1 à 3, à une valeur donnée de $\dot{\gamma}$, pour chacune des sorties. Pour les trois sorties en Méditerranée où des mesures en double ont été effectuées sur les mêmes échantillons, toute la variabilité aurait pu être due à des effets à l'intérieur des échantillons. Des processus floculatifs à l'échelle centimétrique auraient pu être responsables de cette hétérogénéité. L'écart-type gaussien SD_G est constant pour les valeurs les plus élevées de η_E ou de G', où il représente la variabilité (auto-similaire) du milieu. Dans la partie la plus basse, SD_G devient plus élevé, dû probablement à des imprécisions de mesure.

Sur la gamme de $\dot{\gamma}$ ambiante en mer, l'échelle de longueur de turbulence (de Kolmogorov) L a été calculée à partir des viscosités moyennes mesurées. Ces cal-

culs suggèrent que, dans des conditions peu turbulentes ou de forte teneur relative en polymères, L soit plus grande que supposée auparavant et le mélange d'autant moins efficace. La grande valeur de P ainsi que l'hétérogénéité en η_E et en G' augmenterait l'intermittence de turbulence et de mélange. Il est conclu qu'une partie significative de la mer fonctionne comme un gel biopolymérique et grumeleux, dans lequel l'écoulement et le mélange à une échelle $\leq$ 100.L sont sous de fortes influences biologiques.

Oceanologica Acta, 1993. **16**, 4, 317-334.

INTRODUCTION

Old measurements of seawater viscosity (Krümmel, 1907; Miyake and Koizumi, 1948) made at shear rates two to seven orders of magnitude higher than general ambient values (Jenkinson, 1990) are still used in modelling turbulence and calculating energy dissipation in the sea. The Navier-Stokes equations and Kolmogorov's (1941 *a*; *b*) model of turbulence, to which current models of marine turbulence refer, assume the medium to be Newtonian, that is without elasticity and with viscosity independent of shear rate. It has been suggested, however, that easily seen mucus sheaths as well as more dispersed polymers excreted by algae represent increased "structural viscosity", and are used by phytoplankton to manage flow fields (Margalef, 1957; 1978; Hutchinson, 1967; Sournia, 1982; Jenkinson and Wyatt, 1992; Jenkinson, 1993). Moreover adsorption kinetics in natural waters suggest that some filter-passing colloids function as surfaces (Morel and Gschwend, 1987), and must therefore be functionally solid *in situ*. The way ambient viscosity and elasticity vary thus has to be known in order to understand biomodification of flow, dispersion, particle sinking, aggregation/disaggregation (Jenkinson, 1986; Jenkinson *et al.*, 1991; Fogg, 1991), solute dynamics (Morel and Gschwend, 1987) and wave propagation (Saasen and Hassager, 1991).

Offshore, photic-zone concentrations of around 3 g C m^{-3} of dissolved (including most of the colloidal) organic matter (DOM) appear general, of which about 20 % still exceed 100 kdaltons in molecular weight after passing through an injector (Sugimura and Suzuki, 1988). In an imaginary sea devoid of gravitation and flow, aggregates would flocculate out from the dissolved and particulate organic matter (respectively DOM and POM) and continue to grow roughly fractally and indefinitely (Benoit, 1984, cited by Prost and Rondelez, 1991). Even in the real sea, aggregated mucus "clouds" have been seen filling the whole volume between depths of 4 and 9 m over hundreds of square kilometres in the eutrophic northern Adriatic (Stachowitsch *et al.*, 1990). That such networks are able to resist break-up in the tidal waters of the northern Adriatic and that one-metre aggregates roll along the sea bed during current flow (Stachowitsch *et al.*, 1990), with its associated shearing, shows that they impart to the water not only increased viscosity, but also a yield stress (the stress below which the material does not flow, Barnes *et al.*, 1989) at length scales similar to the aggregate dimensions. That bubbles visible to the naked eye are trapped in exceptional algal blooms and in aggregates indicates a yield stress of at least 0.2 Pa (Jenkinson, 1990), while the ability of birds to land on some, perhaps dried, floating aggregates (Stachowitsch *et al.*, 1990) indicates a cm- to dm-scale yield stress of $\geq$ 100 Pa. The negative relationship between excess viscosity and shear rate, found in phytoplankton cultures, suggested to Jenkinson (1986) that the highest values of viscosity at ambient shear rates in the sea might as probably be associated with low-shear deep-ocean water as with higher-shear, near-surface, productive zones rich in DOM.

The objective of the present study was to repeat the old measurements of viscosity in bulk seawater, but at shear rates within the ambient oceanic range, and to measure elasticity at the same time. First, the top 100 m of meso-oligotrophic Mediterranean water was investigated at a single station at four times of year. Shear forces were measured in a rheometer at shear rates from 0.0021 to 0.286 s^{-1}. For comparison, similar measurements were made at shear rates from 0.0021 to 0.973 s^{-1} on sea water taken from a single cruise in shallow waters of the German Bight during patchy plankton blooms. Existing rheometrical and statistical methods were adapted to increase detection limits. In order to correct for mechanical interference of bulk-phase measurements by the surface film, the rheological nature of this surface-film interference was also investigated.

METHODS

Mediterranean study area, sampling and sample handling

Mediterranean samples were obtained at or near a single station about 1 km off the coast in a water depth of ~ 200 m (latitude 43°41'N, longitude 7°21'E) in the rade de Villefranche, France. Appendix Table 1 gives details. Surface slicks and boat wakes were avoided.

Samples of 1 dm^3 were obtained using Van Doorn bottles and immediately transferred to storage bottles through a 0.45 mm mesh. This treatment subjected the water to a shear rate estimated at 10^3 to 3 x 10^3 s^{-1} for several tenths of a second. Within twenty minutes of sampling, the samples were packed in ice, then taken to Grenoble, and their rheology investigated in a temperature-controlled laboratory. Two to four hours before beginning the measurement of each sample, its storage bottle was mixed by gentle inversion, and a subsample of ~ 20 cm^3 poured into a test tube to warm in a water bath set to laboratory temperature. Measurements were made 20 to 48 h after sampling.

Appendix Table 1

Oceanographic data for each Mediterranean cruise.

Données océanographiques pour chaque sortie en Méditerranée.

Date	8 Jul 1986	18 Nov 1986	11 Mar 1987	21 May 1987
Time (GMT)	1230	1650	1320	0900
Depths sampled (m)	0*↗,0**↗,2, 5,10,30,50,75	0↗,2,10,20, 30,50,75,100	0,2,10,20, 30,50,75,100	0,2,5,10,25, 50,75,100
Salinity *in situ* 🗁	37.9-38.3≈	38.1-38.2≈	≈38†	≈38†
Temperature *in situ* 🗁	24.0-14.0≈	17.5-17.1≈	12.8-12.9≈	≈20-≈14†
Density stratification 🕮 [kg m^{-3}]	2.9≈	0.15≈	0.002≈†	1.5≈†
Temperature of measurement (°C)	25 ± 0.5	21 ± 1	22 ± 1	22 ± 1

* - collected at surface 2 m from Villefranche Zoological Station Jetty; ** - not strained; ↗ - sampled by bucket; ≈ - for depths 0-75 m. † - based on data for previous years; 🗁 - From records of Villefranche Zoological station; 🕮 - derived, using tables (Unesco, 1987), from temperature and salinity.

Surface slicks and boat wakes were avoided. Phytoplankton levels were never high (yellow sampling bottle always visible from boat at ≥10 m).

North Sea study area, sampling and sample handling

North Sea samples were obtained on 8 June 1988 at three stations near Helgoland, in depths of water from 15 to 45 m. Stations were selected in which a surface-mixed layer, a principal pycnocline and a bottom-mixed layer were all fairly well defined. Samples were taken by Niskin bottle in these three layers, from the sea-surface microlayer using a glass plate (Harvey and Burzell, 1972), and from the benthic microlayer of amorphous "fluff" using a Reineck box corer. Further details will be given by Jenkinson and Biddanda (in preparation).

Rheometry: theoretical considerations

In sinusoidal deformation (that imposed in *Sinus* mode), the shear rate, $\dot{\gamma}$ varies 90° ahead of the shear γ. In a perfectly elastic solid with negligible viscosity, the shear stress, τ, then varies in phase with the imposed γ. For a Newtonian liquid, by contrast, τ varies 90° ahead of γ (*i. e.* stress and strain are 90° out of phase). For real materials, the elastic and viscous components of resistance to deformation may be separated by resolving the resultant stress into its in-phase and out-of-phase components. The ratio of in-phase stress to applied strain is the elastic modulus, G', while the corresponding parameter for the out-of-phase response is the viscous modulus, G". The energy used in deforming an elastic solid is stored, and then recovered as the sample springs back to its original shape. For a perfect liquid, however, there is no such recovery, and all the energy used in deformation is lost (as heat). Hence G' and G" are also known as the "storage" and "loss" moduli, respectively. The overall response of the sample may be characterized by the complex shear modulus,

$$G^* = [(G')^2 + (G")^2]^{0.5} \quad (1)$$

The viscosity,

$$\eta = G"/\dot{\gamma} \quad (2)$$

The viscosity in some phytoplankton cultures was considered by Jenkinson (1986) to consist of two components such that

$$\eta\,\dot{\gamma}) = \eta_W + \eta_E\,(\dot{\gamma}) \quad (3)$$

where η_W, the viscosity of the aquatic phase, equivalent to the "solvent viscosity" in polymer solutions (Morris, 1984), was independent of $\dot{\gamma}$, while over ± wide ranges of $\dot{\gamma}$ the excess viscosity followed the Ostwald power-law model (Morris, 1984):

$$\eta_E\,(\dot{\gamma}) = k.\dot{\gamma}^{-P} \quad (4)$$

where k and P remain constant. Rheological characterisation was carried out using a *Low Shear 30* rheometer (Contraves AG, Zürich) at the Centre de Recherches sur les Macromolécules Végétales (Centre National de la Recherche Scientifique), the "Grenoble rheometer", and a second rheometer of the same model at the Alfred-Wegener-Institut, Bremerhaven, the "Bremerhaven rheometer".

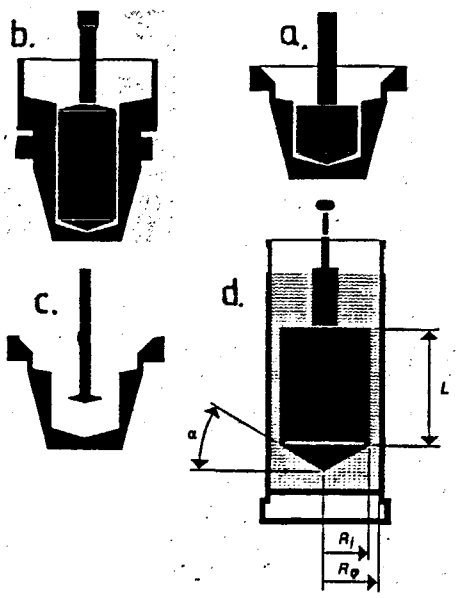

Figure 1

Cross sections of three Couette systems (CS). a) the short CS; b) the tall CS; c) the "surface" CS; d) schematic CS to show dimensions mentioned in Table 1.

Section verticale des trois Systèmes Couette (SC) utilisés. a) le petit SC ; b) le grand SC ; c) le SC pour mesurer la rhéologie de la couche superficielle ; d) schéma d'une SC pour montrer les dimensions données dans le tableau 1.

Table 1

To show dimensions of different Couette systems (CS) used.

Dimensions des différents systèmes de mesure Couette (SC).

Dimension (mm)	Tall CS	Short CS	Surface film CS
L	20.0	8.0	0.0
r_i	5.5	5.5	3.0
r_0	6.0	6.0	6.0
r_{SURF}	12.21	9.37 to 12.0	6.0
r_{STEM}	1.0	1.0	n/a
M'facturer's spec	2T-2T	1-1	1-6

L: height of bob; r_i: radius of bob; r_o: radius of cup in region of bulk-phase measurement; r_{SURF}: radius of cup in region of surface film; r_{STEM}: radius of bob stem; n/a: not applicable.

The sample to be measured was placed in a cylindrical cup, and a bob, suspended coaxially with the cup, was lowered slowly into the test material. This geometry of coaxial cylinders is known as a Couette system (CS). Two geometries of CS were employed, a "tall CS" (Fig. 1 *a*) and a "short CS" (Fig. 1 *b*). To investigate surface effects, a surface bob was used as shown in Figure 1 *c*. Table 1 gives the dimensions of these systems (Fig. 1 *d*).

A sample is sheared by rotating the cup of the CS at a known angular velocity. A shearing force is transmitted across the test sample in the measuring gap (Fig. 1 *a, b*), where it exerts a tangential force on the vertical surface of the bob. This is translated into a torque tending to turn the bob. The instrument reacts to keep the bob from turning by causing an electric current to flow in a coil such that it generates an equal and opposite torque. For a given CS geometry, this current is thus proportional to the torque and hence to the total shear stress, τ. Smaller forces generated by shearing in the bulk material situated between the bottom of the bob and that of the cup, as well as in the upper part of the CS between the bob stem and the upper wall of the cup, are allowed for in the manufacturers' calibration coefficients. The surface film lying between the upper wall of the cup and the bob stem may also transmit tangential forces to the bob stem, and hence torque to the bob. Although surface-film effects are generally neglected in CS measurements, the bulk-phase rheological structure in seawater is much weaker than that generally measured by rheologists. As will be shown, the torque due to surface-film effects therefore interfered with measurements of rheological properties in the bulk liquid, and had to be corrected for.

The rheometers could be operated in two modes, Rotational and *Sinus*. In Rotational mode, the angular velocity of the cup, and hence the shear rate of the test material, $\dot{\gamma}$, could be controlled step-wise, but the cup could be rotated only clockwise. In *Sinus* mode, the cup is rotated back and forth in sinusoidal fashion from - 0.1309 to + 0.1309 rad. This results in a shear, γ, imparted to the test material (assuming no wall slip), oscillating from $-\gamma_{max}$ to $+\gamma_{max}$, where

$$-\gamma_{MAX} = \frac{r_0 + r_1}{2} \cdot \frac{0.1309}{r_0 - r_1} \qquad (5)$$

For both CS systems, the bulk material in the measuring gap is sheared from - 1.505 to + 1.505. Across the gap occupied by the surface film, the shear imposed will not be uniform (Williams and Williams, 1989), but using equation 5 as a guide, γ_{MAX} in the surface film oscillates very roughly from - 0.077 to + 0.077 in the short CS, and from - 0.079 to + 0.079 in the tall CS.

The rheometers were used mostly in *Sinus* mode. As well as a digital display proportional to τ, the instrument produces one analogue output (a voltage) proportional to τ and another proportional to $\dot{\gamma}$. By connecting these two outputs to the x and y channels of a rapid-response, flat-bed graph plotter, a cyclic rheogram ("rhéogramme cyclique", Faurel, 1989) was produced of τ plotted against $\dot{\gamma}$.

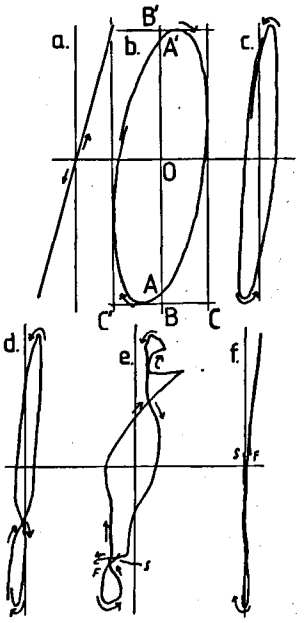

Figure 2

Cyclic rheograms, taken from examples to illustrate: a) type 1, corresponding to Newtonian material; b) type 2, corresponding to linear viscoelastic behaviour, as in a Maxwell fluid (where the viscosity and elastic modulus of the material remain constant during deformation); c) type 3, similar to type 2, except that the plotter pen revolves anticlockwise (see text for explanation); d) type 4.1: pen describes curve showing components of rotation in both directions, in this case a figure-of-eight; e) type 4.2: pen describes a complex curve showing components of rotation in both directions. Vertical axis: $\dot{\gamma}$; horizontal axis: τ (different scales). Letters A, B, B', C, C', O (Fig. b) define line lengths in equations 6, 7 and 8. S, F: start, finish of a plot.

Rhéogrammes cycliques (vrais exemplaires) pour en illustrer : a) type 1, comportement d'un matériau newtonien ; b) type 2, comportement viscoélastique linéaire, par exemple un fluide de Maxwell (où la viscosité et le module élastique restent constants durant la déformation) ; c) type 3, similaire au type 2, sauf que le stylo de la table traçante tourne dans le sens contraire (*voir* le texte pour l'explication) ; d) type 4.1 : le stylo trace une courbe avec des composants de rotation dans les deux sens, dans cet exemple comme un chiffre "8" ; e) type 4.2 : le stylo trace une courbe complexe des composants de rotation dans les deux sens. Axe vertical : $\dot{\gamma}$; horizontal : τ (échelles différentes). Les lettres, A, B, B', C, C', O (Fig. b) définissent les longueurs de lignes dans les équations 6, 7 et 8. S, F : début, fin d'une trace.

Rheograms produced by this system are shown in Figure 2 *a* for a purely viscous liquid, and in Figure 2 *b* for a material showing linear viscoelasticity (one in which η and G' remain constant during the measurement cycle). Other types of curves are produced by materials in which the viscous or elastic modulus changes during the measurement cycle.

For a given CS geometry in which γ is forced to oscillate through a given amplitude and at a given angular frequency, ω, a calibration coefficient, c, is provided. Then,

$$\eta = c \,.\, \sin\delta \,.\, \text{length CB} \quad (6)$$

$$G' = c \,.\, \cos\delta \,.\, \text{length CB} \,.\, \omega \quad (7)$$

where δ is the "loss angle", *i. e.* the phase difference between stress τ and shear γ and the lengths refer to Figure 2 *b*. The cyclic rheogram (Fig. 2 *b*) is used to determine δ as follows (manufacturers' handbooks):

$$\delta = \arccos\left(\frac{\text{length OA}}{\text{length OB}}\right) \quad (8)$$

Williams and Williams (1989) reviewed further theoretical considerations for a variety of geometries and deformational regimes, albeit with much thicker suspensions and higher shear rates in mind.

Rheometry: enhancement of precision

The following precautions were taken to optimize data quality. To reduce air currents at both Grenoble and Bremerhaven, the CS was enclosed in a small Plexiglas box within a larger box protecting the whole rheometer. To reduce vibration, both rheometers were installed on massive microgram-balance-type tables. The Bremerhaven rheometer and its plotter were connected to a stabilized voltage supply, but this was not available at Grenoble, where step-like voltage changes in the mains supply affected the rheograms. Allowance was made for these step-like changes when measuring the rheograms. The plotters were checked and recalibrated when necessary to allow for shrinkage and expansion of the plotting paper caused by humidity changes, and to allow for error due to the lines printed on the graph paper deviating up to 0.5° from the axes of the plotter. With these precautions, and by selecting appropriate expansion of the analogue outputs, a resolution was obtained of 10^{-7} Pa under good conditions of vibration and voltage stability. At Grenoble the laboratory was temperature controlled (extreme limits about ± 0.5°C), and at Bremerhaven the temperature in the CS was maintained constant by a thermostated water jacket (also ± 0.5°C). Since the high-shear viscosity of seawater varies by about 3 % per °C around the temperature of measurement (Miyake and Koizumi, 1948), and the values of η_E, of interest here, are obtained by subtracting η_W from η, better temperature control would probably have considerably improved the precision of measurement of η_E.

Rheometry: calibration of rheometers

No calibration material appears to be available for investigations at the low shear rates, $\dot{\gamma} \geq 2 \times 10^{-3}\ s^{-1}$, and the low shear stresses, $\tau \geq 2 \times 10^{-6}$ Pa, obtained in the present study. I attempted to use freshly double-distilled water as standard, but it generally developed apparent elasticity (probably due to a surface film: *see* below) within two to three hours, the time necessary to cool the sample to constant temperature and carry out a measurement at low $\dot{\gamma}$. Calibration using more viscous materials, such as some calibration oils or glycerol, would have given calibration measurements in which the interference due to surface effects would have been swamped out by components of τ in the bulk material. I rejected the use of these materials for calibration, however, because the values of τ measured for calibration would have been several orders of magnitude higher than those measured in the least viscous samples, and it is doubtful whether such a degree of extrapolation could be justified.

For the rheometer at Grenoble, it will be shown that application of the manufacturer's calibration gave values for η_W between 4.4 and 6.4 % higher than the values given by Miyake and Koizumi (1948) in their Table 2 for η at high $\dot{\gamma}$, η_{MK} (users of this table should beware of some printing errors which become obvious on attempts at critical interpolation.) The manufacturers' calibration has thus been used unchanged for the calculation of viscosity obtained with this instrument.

For the rheometer at Bremerhaven, the viscosity of the least thickened samples was found to vary similarly with shear rate but in a non-linear fashion. This has been interpreted as indicating different degrees of departure from the manufacturers' calibration coefficient for different imposed shear rate, probably due to systematic error in the angular frequency, ω. Calibration was carried out *post facto* using the measurements made on four seawater samples of known salinity which had viscosity low relative to the other samples, and no detectable apparent elasticity. For calibration, it has been conservatively assumed that the mean of the measurements made on these samples corresponds to Newtonian behaviour. These low-viscosity samples included three from the North Sea survey, station

Table 2

Viscosity parameters derived from arithmetically averaged values of viscosity, $\overline{\eta(\dot{\gamma})}$ for each cruise.

Paramètres viscométriques tirés des valeurs moyennes de la viscosité pour chaque sortie en mer, $\overline{\eta(\dot{\gamma})}$.

Cruise	r^2	P	k	η_W (mPa s)	η_{MK} (mPa s)	η_W/η_{MK}
July 1986	0.9999	1.46	0.00021	1.014	0.971	1.044
Nov. 1986	0.9993	1.36	0.00105	1.134	1.068	1.064
Mar. 1987	0.984	1.49	0.00042	1.080	1.015	1.064
May 1987	0.989	1.22	0.0020	1.071	1.015	1.055
North Sea	0.981	1.11	0.045	$0.02 + \eta_{MK}$	Note 1	Note 1

Note 1: η_{MK} variable because of salinity differences. Values given in Appendix, Table 3.

1, 45 m, station 3, 30 m, and station 3, 41 m, and one sample taken from closed, 100 dm^3 container in which seawater had been left to stand undisturbed in a constant-temperature (20°C) room for some days. The salinity of these four samples ranged only from 32.8 to 32.85.

Interpretation of the rheograms obtained

Cyclic rheograms of shear stress, τ, *vs.* shear rate, $\dot{\gamma}$, could be divided into four types. Type 1, illustrated by Figure 2 *a*, corresponded to Newtonian behaviour, that is without any detectable effects of elasticity. Type 2 (Fig. 2 *b*), in which the plotter pen (indicating th $\dot{\gamma}$–τ co-ordinate) revolved clockwise around a rough ellipse, corresponded to visco-elastic behaviour (behaviour due to both viscosity and elasticity). Type 3 rheograms (Fig. 2 *c*) were similar in form to type 2 rheograms, except that the pen rotated *anticlockwise.* In rheograms of type 4, the pen described curves showing both clockwise and anticlockwise components: the pen described either (1) "figures-of-eight" (Fig. 2 *d*) or (2) a curve in which the central part was described by rotation in one direction but loops at one or both extremes were described by rotation in the opposite direction (Fig. 2 *e*); occasional, even more complex rheograms involving components of rotation in both directions were also ascribed to type 4.

To separate surface-film from bulk-phase effects, most samples from the Mediterranean cruises in November, February, and May were measured using both a tall and a short CS. Where the central part of the rheogram showed a clockwise component (type 2 and in some of type 4), the measured storage modulus, G', was assigned a positive value. Where the central part of the rheogram showed an anticlockwise component, however, G' was ascribed a negative value, and for rheograms of type 4 similar in form to figures-of-eight or other complex shapes, G' has been considered unquantifiable, and has been ascribed a default value of zero.

It is frequently recommended that viscosity, $\eta = G''/\dot{\gamma}$, be derived (manufactures' instructions, *see* also Barnes *et al.*, 1989) thus:

$$\eta = [(G^*)^2 - (G')^2]^{0.5}/\dot{\gamma} \quad (9)$$

It will be shown in the Results section, however, that for curves to which G' was ascribed a negative value (criteria given above) the following equation gave better experimental fit:

$$\eta = [(G^*)^2 - G'|G'|]^{0.5}/\dot{\gamma} \quad (10)$$

Equation 10 has thus been used to derive the results of η presented. The review of Williams and Williams (1989) concerns the problems of measuring cohesive, aggregative suspensions, but still at shear rates and stresses much higher than the lowest in the present study.

RESULTS

The complete data set for η and G' is presented for the Mediterranean and the North Sea in Appendix Tables 2 and 3 respectively.

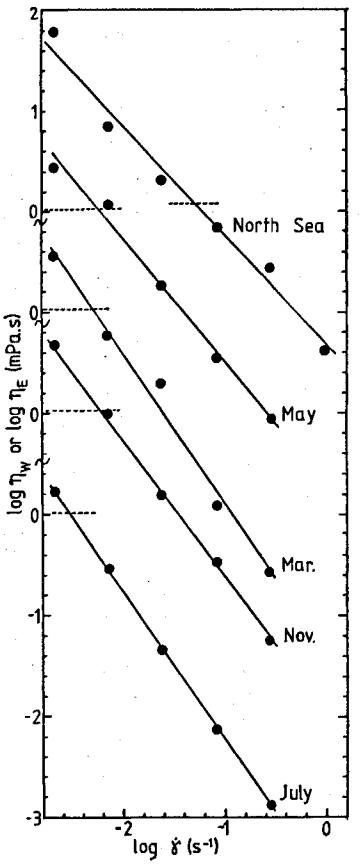

Figure 3

Relationships between $\overline{\eta_E(\dot{\gamma})}$ *and* $\dot{\gamma}$ *for each cruise. Dashed lines:* η_w.

La relation entre $\overline{\eta_E(\dot{\gamma})}$ et $\dot{\gamma}$ pour chaque sortie. En pointillés : η_w.

Viscous components

To test the applicability of the present data of the model expressed by equations 5 and 6, the arithmetic mean of total viscosity $\overline{\eta(\dot{\gamma})}$ was calculated for each shear rate and for each cruise. The value of η_W for each cruise was adjusted to obtain the highest correlation coefficient, r^2, of $\log_{10}(\overline{\eta(\dot{\gamma})} - \eta_W)$ *vs.* $\log_{10}(\dot{\gamma})$. Table 2 shows the values found for r^2, k, P and η_W. For comparison, the viscosity values, η_{MK} proposed by Miyake and Koizumi (1948) for corresponding values of salinity and measurement temperature are also given, as well as values of the ratio η_W/η_{MK}. Figure 3 shows the relationship between $\eta_E(\dot{\gamma})$ and $\dot{\gamma}$. The use of arithmetic means of η_E from a skewed distribution to present overall parameters gives relatively more weighting to viscometric properties in the more viscous samples. These are the samples measured the most precisely. The high resultant values of r^2 support the Ostwald power-law model (equation 6) as a good approximation to the mean viscometric behaviour of the non-Newtonian component in our samples. As shown in Table 2, for all the data from each cruise, P was 1.1 for the North Sea samples and varied from 1.22 to 1.49 for the different Mediterranean cruises. The Mediterranean data represented in Figure 3 were previously published in Jenkinson (1989, Fig. 1 *b*) in preliminary form (calculated using equation 9).

Standard deviation in excess viscosity

Figure 4 shows that as $\dot{\gamma}$ was increased, not only did the standard deviation of the viscosity, SD $[\eta(\dot{\gamma})]$ strongly decrease,

Appendix Table 2

Measured viscosity and storage modulus at shear rates from 0.0021 to 0.286 s^{-1} in Mediterranean seawater samples.

Viscosité et module de conservation mesurés à des vitesses de cisaillement entre 0,0021 et 0,286 s^{-1} dans des échantillons d'eau de mer méditerranéenne.

			Measured viscosity (mPa s)					Measured elastic modulus (μPa)				
C	S	Dep CS	0.0021	0.00716	0.0244	0.0833	0.286	0.0021	0.00716	0.0244	0.0833	0.286
1	1	0 T	1.71	1.087	1.017	0.984	1.000	-0.721	-0.451	-4.36	-3.70	-12.4
1	2	0 T	1.94	1.158	1.12	1.03	1.036	0.2610	1.410ǂ	2.175	0	-2.85
1	3	10 T	N.D.	N.D.	1.067	1.059	1.016	N.D.	N.D.	-2.37	-1.416	-6.510
1	4	20 T	N.D.	1.196	0.979	0.991	0.997	N.D.	0	-0.769	-2.65	-11.0
1	5	30 T	N.D.	N.D.	0.970	1.002	0.997	N.D.	N.D.	-0.167	-2.15	-1.416
1	6	50 T	N.D.	1.35	N.D.	N.D.	N.D.	N.D.	0	N.D.	N.D.	N.D.
1	7	75 T	N.D.	1.42	1.010	1.027	1.038	N.D.	0	-0.2518	-2.20	-5.71
1	8	2 T	4.45	1.761	1.224	1.054	1.020	0.876	1.6470	2.124	0.5645	-5.60
2	1	0 T	0.815	1.355	1.14	1.075	N.D.	0	0	0.2685	0	N.D.
2	2	2 T	1.78	1.20	1.155	1.233	1.150ǂ	0	-1.92	-0.2162	-1.517	-4.228ǂ
2	2	2 S	1.969	1.382	1.181	1.145ǂ	N.D.	0	0	0	0ǂ	N.D.
2	3	10 T	N.D.	1.076	1.182	1.092	1.113	N.D.	0	0	-1.212	-4.225
2	3	10 S	N.D.	1.449	1.142	1.182	1.149	N.D.	0	-0.557	-0.328	-1.09
2	4	20 T	N.D.	1.208	1.151	1.157	1.133	N.D.	0	-0.187	-1.28	-3.22
2	4	30 S	N.D.	1.221	1.162	1.177	1.149	N.D.	0	0	0	0
2	5	30 T	N.D.	1.599	1.163	1.144	1.160	N.D.	1.076	0.8527	0	-2.20
2	5	30 S	N.D.	1.990	1.378	1.189	1.163	N.D.	1.437	0.6727	0.7916	2.206
2	6	50 T	N.D.	1.238	1.156	1.144	1.137	N.D.	0	0	-0.6347	-4.316
2	6	50 S	N.D.	0.966	1.063	1.108	1.102	N.D.	0	0	0	0
2	7	75 T	21.31	6.712	2.711	1.615	1.278	13.76	17.04	7.609	6.29	2.42
2	7	75 S	3.892	1.341	1.213	1.125	1.092	0.0814	0.2556	0.3947	0	0
2	8	100 T	N.D.	1.600	1.217	1.070ǂ	1.042	N.D.	0.07614	-0.3961	-1.478ǂ	-4.95
2	8	100 S	N.D.	2.73	1.299	1.162	N.D.	N.D.	-1.571	-0.8457	-10.45	N.D.
3	1	0 T	3.381	1.246	1.141	1.131	1.110	4.1	3.4	3.8	0	0
3	1	0 S	1.344	1.169	1.142	1.051	1.096	2.0	5.5	0	0	0
3	2	2 T	N.D.	1.166	1.128	1.081	1.098	N.D.	-1.0	-1.003	-1.64	-7.59
3	2	2 S	N.D.	1.639	1.191	1.080	1.075	N.D.	2.97	0.005	0	0
3	3	10 T	N.D.	1.190	1.084	1.060	1.071	N.D.	0	-0.96	-3.22	-2.65
3	3	10 S	N.D.	1.358	2.170	1.112	1.064	N.D.	-14.11	-22.98	-13.20	-14.73
3	4	20 T	1.399	1.226	1.089	1.101	1.141	0	0	-1.0	-3.0	-12.0
3	4	20 S	11.45	2.702	1.111	1.052	1.038	0	11.0	6.0	5.0	1.0
3	5	30 T	1.402	1.142	1.138	1.107	1.091	0.20	0	-0.067	-2.8	-7.5
3	5	30 S	13.81	2.488	1.771	1.209	1.153	80.7	49.7	45.6	38.8	51.1
3	6	50 T	N.D.	1.124	1.088	1.073	1.079	N.D.	0	-1.13	-3.25	-8.48
3	6	50 S	N.D.	1.889	1.352	1.038	1.072	N.D.	-18.57	-18.14	-20.05	-16.70
3	7	75 T	N.D.	1.064	1.134	1.106	1.076	N.D.	0	0	-1.7	-0.8
3	7	75 S	N.D.	1.307	1.092	1.037	1.033	N.D.	0.68	-0.65	0	0
3	8	100 T	1.205	1.286	1.058	1.074	1.073	0	0	-1.0	-4.0	-7.0
3	8	100 S	3.985	0.899	1.044	1.079	1.038	0.5	0	0	-1.2	-20
4	1	0 T	N.D.	1.809	1.089	1.068	1.102	N.D.	0	5.943	0.5745	-4.055
4	1	0 S	N.D.	1.342	0.978	0.893	1.050	N.D.	0	0	0	0
4	2	2 T	1.415	1.125	1.127	1.106	1.093	0.956	0.68	-1.247	-1.786	-14.10
4	2	2 S	4.259	2.509	1.339	1.109	1.081	0	0	0	0	-13.95
4	3	5 T	N.D.	1.112	1.116	1.100	1.100	N.D.	0	0.5449	0	-14.45
4	3	5 S	N.D.	3.144	1.033	1.111	1.072	N.D.	58.69	42.61	56.92	39.16
4	4	10 T	1.287	1.236	1.143	1.106	1.075	0	0	-18.02	-2.976	-19.86
4	4	10 S	1.273	1.089	1.155	1.094	1.058	2.179	5.645	5.916	1.156	-3.824
4	5	25 T	N.D.	1.088	1.101	1.042	1.057	N.D.	0	-1.217	-2.241	-17.57
4	5	25 S	N.D.	3.062	2.497	1.512	1.075	N.D.	165.0	83.88	15.89	36.15
4	6	50 T	0.980	1.387	1.094	1.079	1.078	0	0	0	-3.488	-7.917
4	6	50 S	2.037	2.179	1.209	1.078	N.D.	-11.14	-11.97	-5.762	-3.485	N.D.
4	7	75 T	N.D.	1.213	1.079	1.151	1.086	N.D.	1.040	0	-1.858	-10.0
4	7	75 S	N.D.	4.192	1.064	1.076	1.063	N.D.	-41.20	-16.00	-14.91	-17.66
4	8	100 T	1.041	1.211	1.093	1.042	1.121	0	0	-1.035	-0.578	-18.62
4	8	100 S	1.747	1.919	1.102	1.094	1.064	-18.612	-8.807	-6.464	-10.14	-13.72

ǂ - mean of two measurements.
C - cruise; S - sample no.; Dep - depth (m); CS - Couette system, T (tall) or S (short); N.D. - no data

but so did the ratio SD $[\eta(\dot{\gamma})]/\overline{\eta(\dot{\gamma})}$. This reflects the decreasing importance of $\eta_E(\dot{\gamma})$ (which is intrinsically variable) relative to η_W (which is intrinsically stable) as $\dot{\gamma}$ increases.

To investigate the variation of η_E over different values of $\overline{\eta_E}$ and $\dot{\gamma}$, SD$[\eta(\dot{\gamma})]/\overline{(\eta(\dot{\gamma})}$ has been plotted against $\eta_E(\dot{\gamma})$ (Fig. 5). The curve "hugs" the upper side of a straight line representing SD$[\eta_E(\dot{\gamma})] = \overline{\eta_E(\dot{\gamma})}$ with ratios of SD$[(\eta(\dot{\gamma})]/\overline{\eta_E(\dot{\gamma})}$ mostly between 1 and 3, irrespective of $\dot{\gamma}$, except at values of $\eta_E(\dot{\gamma})$ below ≈ 100 μPa s. Below this excess viscosity, the curve "peels away" from the straight line, SD $[\eta(\dot{\gamma})] = \overline{\eta_E(\dot{\gamma})}$, to give higher values of SD $[\eta(\dot{\gamma})]/\overline{\eta_E(\dot{\gamma})}$, the highest recorded being ≈ 13 at $\overline{\eta_E(\dot{\gamma})} = 1.3$ μPa s. This represents a higher relative importance of errors in η when η is low. Possible sources of these errors may include: 1) imprecision in the instrument, in the plotter and in measurements made of the plotted output; 2) in Mediterranean samples only, variation in salinity acting on

Appendix Table 3

Measured viscosity and storage modulus at shear rates from 0.0021 to 0.973 s^{-1} in North Sea seawater samples.

Viscosité et module de conservation mesurés à des vitesses de cisaillement entre 0,0021 et 0,973 s^{-1} dans des échantillons d'eau de mer de la Mer du Nord.

			η_{MX} (mPa s)	Measured viscosity (mPa s)					Measured elastic modulus (μPa)					
S	L	Dep		0.0021	0.00716	0.0244	0.0833	0.286	0.973	0.0021	0.00716	0.0244	0.0833	0.286	0.973
1	1	0	1.217	1.758	1.366	1.107	1.032	1.242	1.248	0.24	3.2	8.9	28	30	64
1	2	3	1.217	N.D	1.787	1.331	1.282	1.245	1.235	N.D	2.2	0.31	2.1	0.0	-8.7
1	3	12	1.216	N.D	1.365	1.276	1.304	1.282	1.257	N.D	0.0	0.65	7.1	0.0	-5.9
1	4	30	1.216	N.D	1.338	1.238	1.198	1.247	1.246	N.D	0.0	0.0	0.0	0.0	12
1	5	45	1.218	1.225	1.242	1.303	1.239	1.241	1.235	0.0	0.0	0.0	0.0	0.0	0.0
2	1	0	1.207	16.11	3.997	1.873	1.505	1.248	1.219	7.1	12	8.5	10.0	12	7.8
2	2	3	1.207	N.D	3.472	1.470	1.337	1.327	1.262	N.D	2.5	0.52	0.0	0.0	-24
2	3	8	1.210	N.D	2.184	1.361	1.284	1.257	1.225	N.D	1.0	1.6	2.8	0.0	0.0
2	4	14	1.213	N.D	10.93	2.234	1.279	1.251	1.268	N.D	23	21	20	0.0	-33
2	4	14	1.213	145.3	59.49	21.58	9.653	3.893	1.488	133	255	344	523	629	480
2	5	15	1.213	N.D	1.837	1.192	1.257	1.282	1.224	N.D	0.87	0.0	0.0	0.0	0.0
3	1	0	1.218	15.36(1)						15(1)					
3	1	0		42.66(2)						67(2)					
3	1	0		156.8(3)	46.04	14.31	3.603	2.608	N.D	207(3)	209	216	138	154	N.D
3	1	0	1.218	N.D	1.591	1.117	1.213	1.208	1.224	N.D	0.0	0.0	0.0	0.0	0.0
3	2	3	1.218	N.D	1.336	1.257	1.223	1.222	1.230	N.D	0.31	0.0	0.0	0.0	-8.6
3	3	10	1.218	N.D	1.273	1.238	1.206	1.246	1.240	N.D	0.0	0.0	0.0	0.0	-32
3	4	30	1.218	N.D	1.258	1.191	1.244	1.212	1.214	N.D	0.0	0.0	0.0	0.0	0.0
3	5	41	1.218	N.D	1.178	1.219	1.263	1.260	1.263	N.D	0.0	0.0	0.0	0.0	0.0

Notes: (1) - first measurement; (2) - after 100 minutes in CS; (3) - after 9 hours in CS.
Abbreviations: S - station no.; L - layer (1 - surface microlayer; 2 - upper mixed layer; 3 - main pycnocline; 4 - lower mixed layer; 5 - benthic microlayer of organic "fluff"); Dep - depth (m); N.D - no data; η_{MX} - viscosity of seawater at salinity measured *in situ* and temperature in the rheometer (15°C), according to Miyake and Koizumi (1948); salinity of benthic microlayer assumed to be that of overlying water.

η_W; 3) variation in measurement temperature acting on η_W; 4) a confounding effect due to variation in P. In comparison, the manufacturers' specifications (Bulletin T321f-8201CZ, Contraves AG) give ≤ 2 % for instrument "[im]précision", representing about 20 μPa s when $\eta_E << \eta_W$.

It is concluded that when 100 μPa s < η_E < 100 mPa s, variance due to experimental imprecision is low. The fairly constant value of d[SD (η)]/d($\overline{\eta_E}$) over three orders of magnitude in $\eta_E(\dot{\gamma})$ as well as over one order of magnitude in $\dot{\gamma}$, indicates that the variation in excess viscosity was self-similar over these ranges of $\eta_E(\dot{\gamma})$ and $\dot{\gamma}$.

Figure 4

Mean, standard deviation (SD) and 2 x standard error (SE) (approximately 95 % confidence limit) for viscosity (η) as well as SD(η)/mean(η), plotted for each shear rate and cruise. Note that vertical scale for the North Sea cruise is five times that for the Mediterranean cruises.

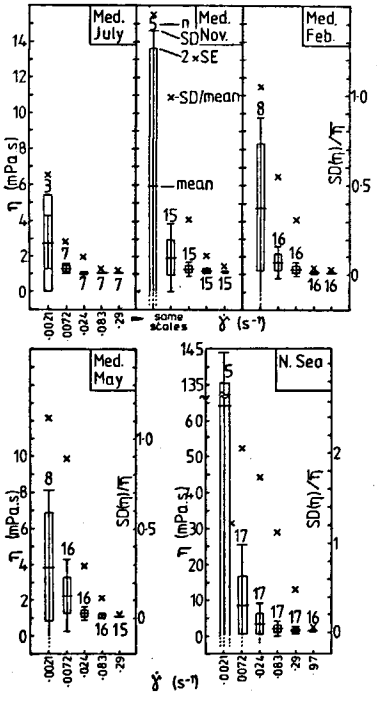

Moyenne, écart-type (SD) et 2 x écart-type de la moyenne (SE) (limite de confiance 95 % approximativement) pour la viscosité (η) ainsi que SD(η)/moyenne(η) pour chaque vitesse de cisaillement et pour chaque sortie. Noter que l'échelle verticale pour les données de la Mer du Nord est cinq fois supérieure à celle des données méditerranéennes.

Elastic components in the Mediterranean samples

In Figure 6 measured elastic modulus G' is plotted against measured excess viscous modulus, $G''_E = \eta_E.\dot{\gamma}$, for all measurements where G' ≠ 0. There is considerable clustering of points around the origin, and there were 107 cases where G' was negative and 61 where it was positive (plus 71

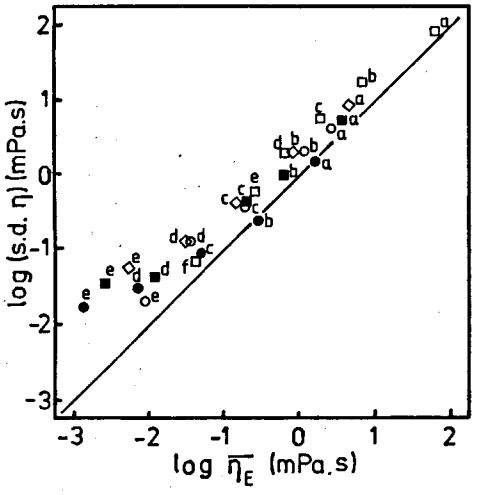

Figure 5

Log-log plot of SD(η) vs.$\overline{\eta_E}$ for each cruise and each shear rate. The straight line represents SD(η) =.$\overline{\eta_E}$ for comparison. Mediterranean cruises: ●: July 1986; ✧: November 1986; ■: March 1987; ○: May 1987. North sea cruise:□:June 1988. Shear rates (s^{-1}); a: 0.0021; b: 0.00716; c: 0.0244; d: 0.0833; e: 0.286; f: 0.973.

La relation logarithmique de SD(η) avec.$\overline{\eta_E}$ pour chaque sortie et pour chaque vitesse de cisaillement. La ligne droite représente SD(η) =.$\overline{\eta_E}$. Les sorties en Méditerranée : ● : juillet 1986 ; ✧ : novembre 1986 ; ■: mars 1987 ; ○ : mai 1987. Sortie en Mer du Nord : □ : juin 1988. Vitesses de cisaillement (s^{-1}); a : 0,0021 ; b : 0,00716 ; c : 0,0244 ; d : 0,0833 ; e : 0,286 ; f : 0,973.

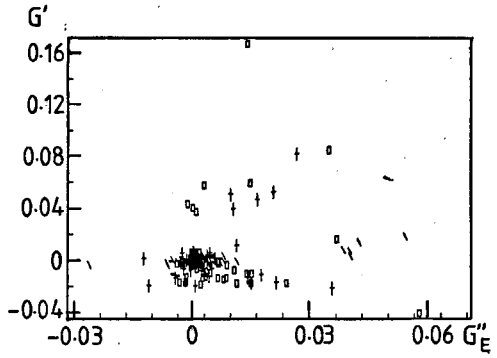

Figure 6

Measured G' vs. measured G"$_E$ for all Mediterranean measurements. ■ : July 1986; \: November 1986; +: March 1987; □: May 1987.

La valeur mesurée de G' *vs.* celle de G"$_E$ pour toutes les données de la Méditerranée. ■ : juillet 1986 ; \ : novembre 1986 ; + : mars 1987 ; □-: mai 1987.

cases where G' was classed as zero). For the set of data points in which G' ≠ 0, the largest absolute values of the measured elastic modulus, |G'|, however, represented positive G'. In order to compare independent data points, $\overline{G'}$ has been compared with $\overline{G''}$ (where the overbar signifies the mean of all measurements for each sample) for samples in which $\overline{G'} \neq 0$. While there was no correlation discernible between $\overline{G'}$ and $\overline{G''_E}$, correlation was significant between $\overline{|G'|}$ and $\overline{G''_E}$ [$r^2 = 0.28$; $0.000\,05 < P < 0.0001$ (distribution not illustrated)]. Furthermore, if (for reasons explained in the following section) |G'| is multiplied by 2.24 for sets measured using the tall CS, the closeness of the relationship is improved ($r^2 = 0.36$; $0.000\,001 < P < 0.000\,005$).

Tests of whether surface-film or bulk-phase effects were responsible for the measured rheological properties

Because the area of the side of the bob bordering the measuring gap (the surface on which measured bulk-phase forces act) is greater in the tall CS than in the short one, while other dimensions (particularly the width of the measuring gap and the diameters of both the bob and of the bob stem) are identical (Fig. 1 *a*, *b*), the manufacturers' calibration sheets indicate that a given tangential force exerted by the surface film on the bob stem, producing the same torque in both CS systems, is equivalent to a bulk-phase shear stress, τ, 2.24 times greater in the small CS than in the tall one. Where $\overline{comp(S)}$ and $\overline{comp(T)}$ are, respectively, the mean of any rheological component measured in the small CS and the tall CS (and calculated from calibration coefficients for bulk-phase components), a rheological component due exclusively to bulk-phase effects should give $\overline{comp(S)}/\overline{comp(T)} = 1$, while one due exclusively to surface-film effects should give $\overline{comp(S)}/\overline{comp(T)} = 2.24$.

Figure 7 shows the excess viscous modulus measured in the tall CS, $\overline{G''_E(T)}$, plotted against that for the same sample measured in the small CS, $\overline{G''_E(S)}$. An obvious absence of correlation is indicated between $\overline{G''_E(T)}$ and $\overline{G''_E(S)}$. To carry out statistical analysis on independent variables, $\overline{G''_E(T)}$ was plotted against $\overline{G''_E(S)}$ (Fig. 8). The overall

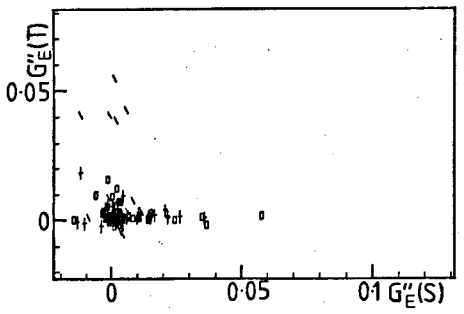

Figure 7

For cruises 2, 3 and 4, G"$_E$ measured in the tall CS vs G"$_E$ measured in the small CS. All pairs of measurements (for cruise 1, measurements not made using the small CS).

Pour les sorties 2, 3 et 4, la distribution des paires : G"$_E$ mesuré avec le grand système Couette (SC) *vs.* G"$_E$ mesuré avec le petit SC. Toutes les paires de mesures sont indiquées (pour la sortie 1, des mesures n'ont pas été faites avec le petit SC.)

mean of $\overline{G''_E(T)}$ 3.2 μPa (SD 9.1) was not significantly different from that of $\overline{G''_E(S)}$ 5.0 μPa (SD 7.0), as determined by Student's paired t-test ($n = 23$). It is thus concluded that the relationship is statistically compatible with the hypothesis that all the excess viscosity was contributed by bulk-phase effects.

By contrast, the same overall mean of $\overline{G''_E(T)}$, 3.2 μPa (SD 9.1) is significantly smaller than that of the overall mean of $\overline{G''_E(S)}$. 2.24, 11 μPa (SD 16) ($0.01 < P < 0.05$; $n = 23$). It is thus concluded that this relationship is not compatible with a hypothesis that all the excess viscosity was contributed by the surface film. There was no significant correlation or slope in either of the above graphs, indicating no significant relationship between excess viscosity in pairs of measurements (using the tall CS and the small CS) made on the same sample. The intercept, 4.6 μPa (95 % confidence limit ± 3.8) was significantly > 0, simply reflecting that the overall mean of $\overline{G''_E(T)}$ is significantly > 0.

Proceeding similarly for the measured elastic modulus, Figure 9 *a* shows $\overline{G'(T)}$ plotted against $\overline{G'(S)}$. There is no significant correlation or slope. The overall mean of

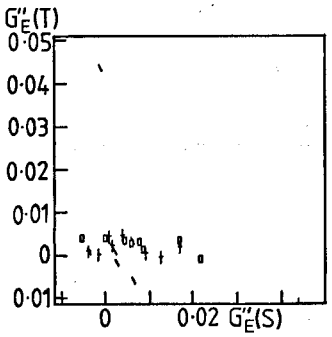

Figure 8

For cruises 2, 3 and 4, the mean value of G"$_E$ (at all the shear rates employed for each sample) measured in the tall CS vs. mean G"$_E$ measured in the small CS (for cruise 1, measurements not made using the small CS).

Pour les sorties 2, 3 et 4, la valeur moyenne de G"$_E$ (à toutes les vitesses de cisaillement utilisées pour chaque échantillon) mesurée avec le grand SC *vs.* la moyenne de G"$_E$ mesurée avec le petit SC (pour la sortie 1, des mesures n'ont pas été faites avec le petit SC.)

$\overline{G'(T)}$ - 3.1 μPa (SD 7.4) is (of opposite sign but) only marginally significantly different from that of $\overline{G'(S)}$, + 4.4 μPa (SD 25.4) ($0.05 < P < 0.1$; n = 46), while SD[$\overline{G'(T)}$] is less than SD[$\overline{G'(S)}$] by a factor of 3.4. Plotting $\overline{G'(T)}$.2.24 against $\overline{G'(S)}$ (Fig. 9 *b*), the overall means are now significantly different ($0.01 < P < 0.05$; n = 46).

Figure 10 *a* shows $|\overline{G'_T}|$ plotted against $|\overline{G'_S}|$. Again there is no significant correlation or slope. The overall mean of $|\overline{G'_T}|$, 5.3 μPa (SD 6.0), is significantly less than that of $|\overline{G'_S}|$, 16 μPa (SD 20), ($0.0005 < P < 0.0001$; n = 46) by a factor of 3.04. This result is not compatible statistically with a hypothesis that all the measured positive and negative elasticity could have been contributed by the bulk phase. Figure 10 *b* shows ($|\overline{G'_T}|$ x 2.24) plotted against $|\overline{G'_S}|$. The overall mean of ($|\overline{G'_T}|$x 2.24) 11.8 μPa (SD 13.5), is still less than that of $|\overline{G'_S}|$ (unchanged), now by a factor of 1.36, but the difference is not significant. This result is compatible statistically with the hypothesis that all the measured positive and negative elasticity was contributed by the surface film. As with the excess viscous modulus, G''_E, no significant correlation was found between duplicate measurements (tall and small CS) of the same samples, in either G' or |G'|.

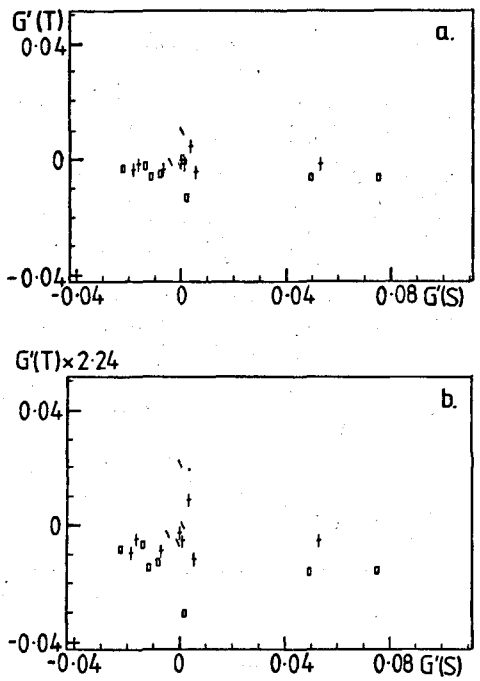

Figure 9

For cruises 2, 3 and 4: a) comparison between CS geometries. The mean value (measured at all the shear rates employed for each sample) of the elastic modulus in the tall CS, $\overline{G'(T)}$ vs. *mean of that measured in the small CS, $\overline{G'(S)}$ (statistically identical values should be expected if elastic modulus due only to bulk phase): b) same comparison but with $\overline{G'(T)}$ multiplied by 2.24; (statistically identical values should be expected if elastic modulus due only to surface phase; for cruise 1, measurements not made using the small CS).*

Pour les sorties 2, 3 et 4 : a) comparaison entre les deux géométries de SC. La valeur moyenne (mesurée à toutes les vitesses de cisaillement utilisées pour chaque échantillon) du module élastique avec le grand SC, $\overline{G'(T)}$ *vs.* la moyenne de celui mesuré avec le petit SC, $\overline{G'(S)}$; (des valeurs identiques seraient à prévoir si le module élastique provenait uniquement de la phase volumique). b) la même comparaison, mais en multipliant $\overline{G'(T)}$par 2,24.(des valeurs identiques seraient à prévoir si le module élastique provenait uniquement de la phase superficielle ; pour la sortie 1, aucune mesure n'a été faite avec le petit SC.)

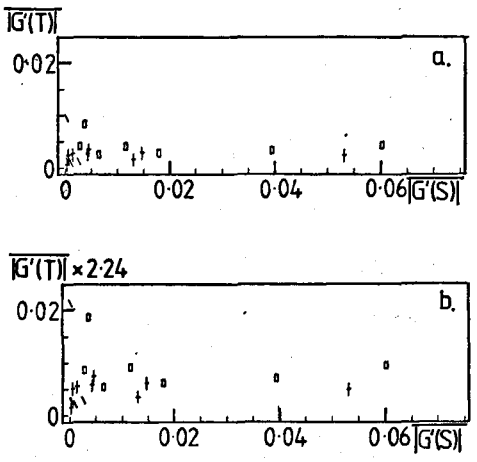

Figure 10

As Figure 9, but comparisons of the means (at all shear rates employed) of absolute values of the elastic moduli $|\overline{G'(T)}|$ and $|\overline{G'(S)}|$.

Comme la figure 9, sauf que ce sont les moyennes (sur toutes les vitesses de cisaillement utilisées pour chaque échantillon) des valeurs absolues de modules élastiques $|\overline{G'(T)}|$ et $|\overline{G'(S)}|$ qui sont comparées.

From these statistical considerations alone, it can be deduced that: 1) surface-film effects were responsible for much or all of the measured elasticity; 2) surface-film effects were responsible for none or some of the measured excess viscosity, but not all of it; 3) bulk-phase effects were responsible for none or some of the measured elasticity, but not all of it; 4) bulk-phase effects were responsible for some or all of the measured excess viscosity.

The absence of any discernible correlation between duplicate measurements (tall and small CS) of either viscosity or elasticity suggests that measured rheological variation within the Mediterranean cruises was dominated by within-sample heterogeneity.

Investigation of surface effects with a surface CS

Surface effects were measured at Bremerhaven using a surface bob (Fig. 1 *c*). Figure 11 shows the results obtained for the surface film of deionized double distilled water (DDDW) which had been kept in a laboratory wash bottle for several days. The surface shear stress, τ_{SURF}, oscillated with the same frequency as that of cup rotation and with a half-amplitude ≈ 0.03 mN m^{-1} (Fig. 11). The mean value and the amplitude of τ_{SURF} were both practically independent of cup rotation speed and hence of surface shear rate $\dot{\gamma}_{SURF}$. Oscillation was quasi-sinusoidal except for some pre-peak instability (arrowed in Fig. 11), indicating yielding in the film or slipping at its edge.

With filtered *Skeletonema* culture, quasi-sinusoidal oscillation in τ_{SURF} also occurred, but no instability was discernible. On standing of this culture in the CS (between measurements), the amplitude of oscillation in τ_{SURF} showed a quasi-exponential increase with time. This increase may reflect adsorption of bulk-phase polymers on to the surface, and perhaps also chemical or microbiological network formation.

Oscillation did not occur when the procedure was carried out with any CS system when it was empty, indicating that magnetism in the CS was not responsible.

Whatever the mechanism responsible for the oscillation in τ_{SURF} (this is treated further in the "Discussion"), it is likely that tangential forces of a similar type acted also on the stems of the bobs used in *Sinus* mode for the bulk-phase measurements (the tall CS and the short CS).

Assuming that shear is uniform across the surface from the wall of the CS cup to the edge of the surface-phase bob and neglecting any effects produced by the meniscus or by variations in the amount the short CS was filled on the wall-to-bob distance, shear rate in the surface film, $\dot{\gamma}_{SURF}$, was then 1/16 to 1/22 shear rate in the measuring gap. In practice, values are likely to be higher near the bob stem (Barnes *et al.*, 1989).

If the imposed shear, γ, was oscillated sinusoidally over a part of the curve of torque *vs.* rotation with positive slope (illustrated in Fig. 12 by Bar D), then even in the absence of bulk-phase elasticity, a trace of τ *vs.* $\dot{\gamma}$ would rotate clockwise (Inset D), giving a positive value for measured apparent elasticity. If, however, γ was oscillated over a part of the curve with negative slope (Bar C, Inset C), the trace would rotate anticlockwise, giving negative apparent elasticity. If γ was oscillated over a part showing a maximum or a minimum (Bars A,B; Insets A,B) the curves illustrated would result. Traces resembling figures-of-eight are likely to result where the change in direction of rotation affected the curve of τ in relation to CS position (both clockwise and anticlockwise plots were in fact obtained in *Sinus* mode using the surface bob.)

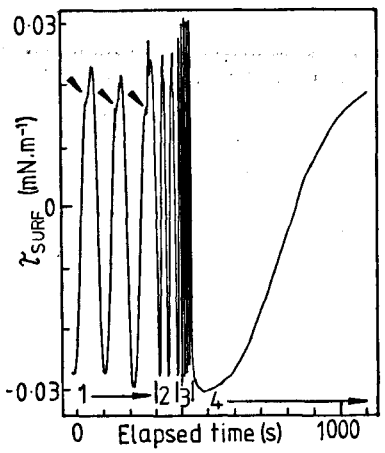

Figure 11

Linear rheogram, in which torque is plotted against time during uniform rotation of the CS cup. Surface bob (Fig. 1 c). Double-distilled water after several days' storage in wash bottle, followed by several hours in CS, 20°C. Rotation speeds (min^{-1}) and surface shear rates (s^{-1}) during marked periods: 1-0.53, 0.093; 2-1.81, 0.32; 3-6.2, 1.08; 4-0.013, 0.0023. Each oscillation of the surface shear stress, τ_{SURF}, was found to correspond exactly to one revolution of the CS cup. Arrows indicate probable surface-film yield or wall slip. The position of the zero on the vertical axis is arbitrary.

Rhéogramme linéaire, dans lequel est indiquée l'évolution du moment de rotation. Rotation uniforme du godet du SC. Corps de mesure superficiel (*voir* Fig. 1 *c*). Eau bidistillée, après quelques jours dans une pissette suivis de quelques heures dans le SC (20°C). Vitesses de rotation (min^{-1}) et vitesses de cisaillement de surface (s^{-1}) durant les périodes marquées : 1-0.53, 0.093 ; 2-1.81, 0.32 ; 3-6.2, 1.08 ; 4-0.013, 0.0023. Chaque oscillation de la contrainte de cisaillement de surface, τ_{SURF}, correspondait de façon précise à une révolution du godet du SC. Les flèches indiquent ce qui est probablement une déformation permanente de la couche superficielle ou un glissement de celle-ci à la paroi. La position du zéro sur l'axe vertical est arbitraire.

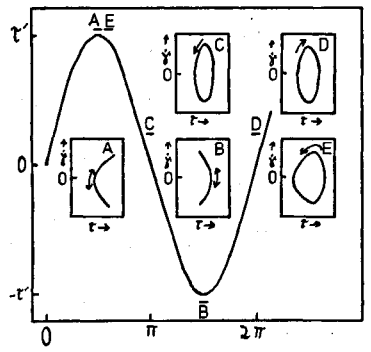

Figure 12

Suggested mechanism for producing observed surface-film effects. In rotational mode, force, τ_{SURF}, produced on the bob stem by surface effects, varies sinusoidally with rotation of the cup. Horizontal bars under letters represent the amplitude of back-and-forth rotation (- 7.5° to + 7.5°) in Sinus *mode. Inserts show the cyclic rheograms which would be produced by centring this back-and-forth rotation at different amounts of rotation. Assuming that no hysteresis occurs during this back-and-forth scanning (hysteresis could only be due to energy dissipated in the surface film) the curve of τ_{SURF} above the horizontal line of $\dot{\gamma}$ = 0 will be a mirror image of that below this line, and should not produce any falsification of calculated bulk-phase viscosity, η. A false component would be produced, however, in the measured bulk-phase elastic modulus, G'. For instance, inset D would wrongly indicate a positive measured value of G', while insets C and E would both indicate negative values. Any hysteresis or instability in τ_{SURF} during back-and-forth rotation should add further false variance to calculated values of G' and η.*

Mécanisme suggéré de la production des effets de couche superficielle. En mode rotatif, la force τ_{SURF}, produite sur la tige du corps de mesure où elle coupe la surface de l'eau dans le godet, varie de manière sinusoïdale durant la rotation du godet. Les barres horizontales dessinées sous les letres indiquent l'ampitude de l'oscillation rotative (- 7,5° à + 7,5°) en mode *Sinus*. On montre en encadrés les rhéogrammes cycliques qui seraient produits à différents points où cette oscillation pourrait être centrée. Dans le cas d'aucune hystérésis (qui serait due à la perte d'énergie dans la couche superficielle), la courbe de τ_{SURF} au-dessus de la ligne horizontale, $\dot{\gamma}$ = 0, serait l'image de celle au-dessous de cette ligne, et ne fausserait pas le calcul de la viscosité de la phase de masse, η. Cependant, un faux composant dans la valeur mesurée du module élastique de masse, G', serait à prévoir. Par exemple, l'encadré D indiquerait faussement une valeur positive de G', tandis que les encadrés C et E en indiqueraient des valeurs faussement négatives. Toute hystérésis ou instabilité en τ_{SURF} pendant le balayage ajouterait en plus une variance faussement augmentée aux valeurs mesurées de G' et de η.

The largest amplitudes of torque encountered represented tangential forces of 0.17 mN m^{-1} (distilled water), 0.034 mN m^{-1} (0.2 µm filtered sea water) and 2.0 mN m^{-1} (filtered *Skeletonema* culture). Measurements carried out using the surface bob in *Sinus* mode using both the filtered sea water and the filtered *Skeletonema* culture, gave curves characteristic of positive or negative elasticity but without viscosity.

Elastic components in the North Sea samples

The measured values of G' (Appendix Tab. 3) are plotted against G"$_E$ in Figure 13. Those values of G' obtained at $\dot{\gamma}$

= 0.973 s^{-1} are thought to be contaminated by interaction among rheological properties, inertial effects in both the bob and the test material, and finite reaction time of the torque-plotting system. The viscosity values (obtained by correction using the possibly erroneous values of G') seem reasonable, however.

Excluding data obtained at $\dot{\gamma}$ = 0.973 s^{-1}, no North Sea sample showed negative measured G', while 35 positive values were obtained, suggesting that the mechanisms contributing to measured G' in the North Sea samples were different from those in the Mediterranean water. That the North Sea data were all obtained with the same CS geometry has precluded statistical tests similar to those carried out on the Mediterranean water, to determine whether surface or bulk effects were responsible.

Comparison of Figure 13 with Figure 6 shows that some of the values of both G''_E and G' (maxima 700 and 600 µPa respectively) were an order of magnitude higher than the highest found in the Mediterranean samples (corresponding maxima 40 and 80 µPa). Figure 13 shows the positive relationship between G''_E and G'. This relationship is contributed only by the higher values, the cluster of points near the origin (Fig. 13 inset) showing no such strong relationship.

Rank-value distributions of measured rheological properties

The Zipf-Mandelbrot log(rank)-log(frequency) distribution is frequently used to illustrate the distribution of organisms among the different taxa in an assemblage (or in a sample) (Frontier and Pichod-Viale, 1991). The rank of the most abundant taxon is scaled as unity. We have adapted this type of plot to illustrate the distribution of parameter values in any set of them. Sets with different numbers of values are rendered comparable by dividing rank by the number of data points in the set, giving a plot of log(rank/n) *vs.* log(parameter value). Using this plot for values of measured G''_E and G', negative measured values [as log(- value)] are shown separately, but n is the total number of samples (negative, zero and positive) in the set. In both the rank-frequency plot and the rank-value plot the slope of the graph represents the Gaussian standard deviation, SD_G. How SD_G varies with rank is thus obvious from the plot.

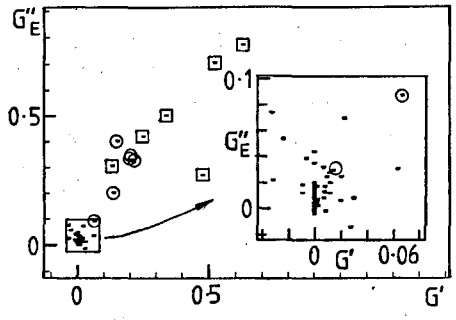

Figure 13

For the North Sea cruise, for all samples, and measurements at all shear rates (including $\dot{\gamma}$ = 0.973 s^{-1}). G' vs G''_E. Main graph: all the data. Inset : "window" around the origin. Correlation, r = 0.973, G' = 0.735[± 0.06].G''_E - 0.005[± 0.008] [95 % confidence limits]. As seen in the inset, however, the two samples with the highest values of G' and G''_E (data points surrounded by squares and circles) produced practically all this correlation (all negative values of G' were obtained at $\dot{\gamma}$ = 0.973 s^{-1}).

Pour la croisière en Mer du Nord, pour tous les échantillons et pour toutes les vitesses de cisaillement (y compris $\dot{\gamma}$ = 0,973 s^{-1}), G' *vs.* G''_E. Figure principale : toutes les données. En médaillon : "fenêtre" autour de l'origine. Corrélation, r = 0,973, G' = 0,735[± 0,06].G''_E - 0,005[± 0,008] [limites de confiance à 95 %]. Cependant, seules les deux échantillons dotés des valeurs les plus importantes de G' et de G''_E (données entourées d'un carré ou d'un cercle) ont produit la plupart de cette corrélation (toutes les valeurs négatives de G' ont été mesurées à $\dot{\gamma}$ = 0,973 s^{-1}).

The two variables presented are $\overline{G''_E}$ (Fig. 14 *a*) and $\overline{G'}$ (Fig 14 *b*), where the overbar signifies the arithmetic mean in measurements of a sample at all values of $\dot{\gamma}$ (in these cases, excluding $\dot{\gamma}$ = 0.973 s^{-1}). Series of measurements carried out in the tall CS and the short CS (Mediterranean study) are treated as separate samples since they showed no correlation, as are measurements on duplicate samples (some North Sea samples).

Three out of the four Mediterranean samples with the highest mean excess viscous modulus, $\overline{G'_E}$, were also among the four samples with the highest values of the mean elastic modulus, $\overline{G'}$. Similarly, six of the seven North Sea samples with the highest values of $\overline{G'_E}$ were among the seven with the highest values of $\overline{G'}$, and their respective rank orders were almost the same (Fig. 14 *a*, *b*). In the seven North Sea samples with the highest values of $\overline{G''_E}$ and $\overline{G'}$, the ratio $\overline{G'}/\overline{G''_E}$ varied only from 0.23 to 0.72, indicating that similar polymers may have caused most of the viscous and elastic thickening. That values of $\overline{G'}$ in the Mediterranean are in the majority negative suggests that a systematic negative error was introduced by the measurement technique, perhaps due to a lag in stress output relative to that of the CS position output in the rheometer-recorder system. That negative values of G' occurred only at $\dot{\gamma}$ = 0.973 s^{-1} in measurements of the North Sea samples (despite likely positive and negative surface-film errors) supports this suggestion. The four largest absolute values of $\overline{G'}$ measured in the Mediterranean samples were all positive, however, suggesting that bulk-phase elasticity was dominating both that due to surface effects and that due to systematic measurement error in measured values of G' in these samples. The ratios of $\overline{G'}/\overline{G''_E}$ ranged from 0.22 to 11.2 in these samples suggesting that the material contributing to the bulk-phase rheological properties in the Mediterranean samples was structurally more diverse than that in the North Sea samples. That excess viscosity in the North Sea samples was closely correlated with chlorophyll content mostly due to *Phaeocystis* blooms (Jenkinson and Biddanda, in preparation) suggests that this material comprised mainly exopolymers derived from a single species.

The rank-value diagram of $\overline{G''_E}$ (Fig. 14 a) resembles a straight line of slope - 0.9 from ranks 1 (+ 43 µPa) to 33 (+ 1.6 µPa) for the Mediterranean samples, while for the North Sea data set the curve approximates also to a straight line, but less closely, from ranks 1 (+ 540 µPa) to 9 or 10 (≈ + 2 µPa), with a slope of - 2.6. At higher values of scaled rank, the slope increases rapidly for both

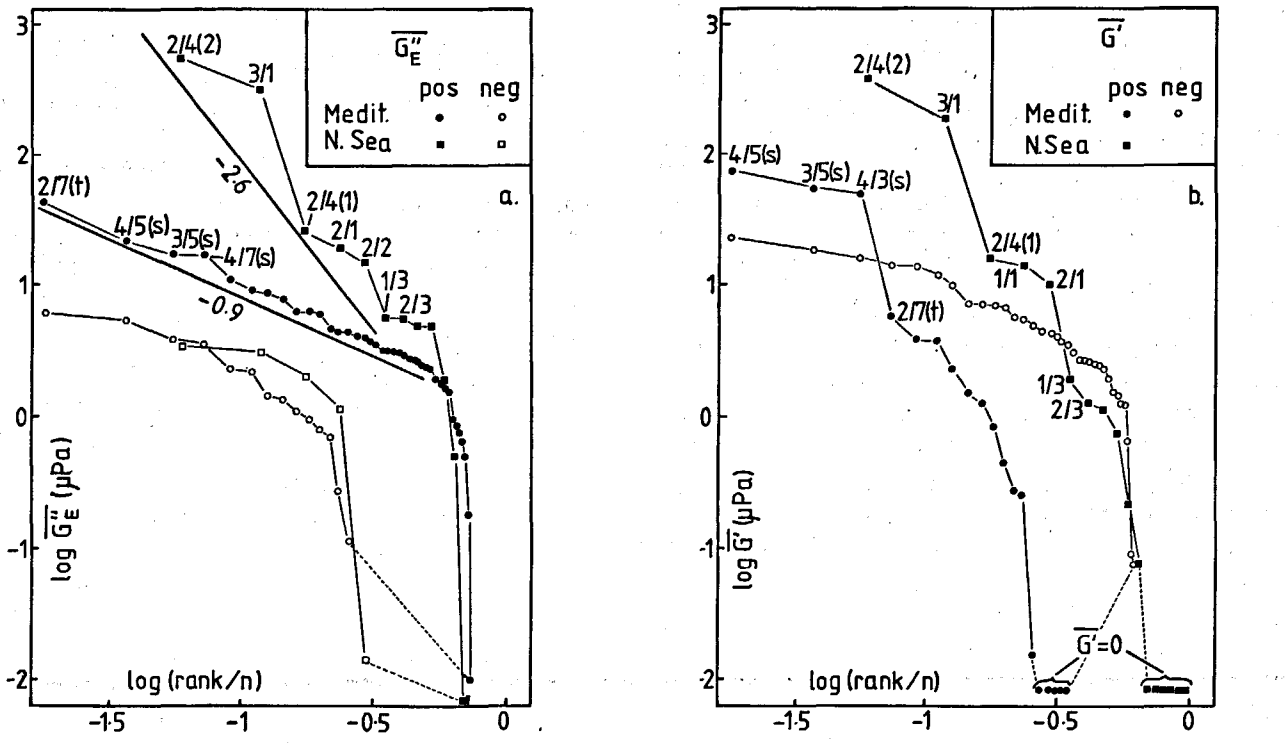

Figure 14

Zipf-type graphs of elastic and excess viscous moduli vs. *(sample rank/total number of samples). Duplicate subsamples are treated as separate samples. Logs of both positive and negative measured values are plotted, using different symbols, and values of zero are indicated separately. The scale of the horizontal axis is twice that of the vertical one. a) mean (over all shear rates for each sample) excess viscous modulus, $\overline{G''_E}$; b) mean elastic modulus, $\overline{G'}$ (any values measured at $\dot{\gamma}$ = 0.973 s^{-1} excluded from mean).*

Courbes de type Zipf du module élastique et du module visqueux excédentaire *vs.* (rang de chaque échantillon/nombre d'échantillons). Des mesures de sous-échantillons sont comptées comme d'échantillons à part entière. Les logarithmes des valeurs positives, zéro et négatives sont indiqués avec des symboles différents. L'axe vertical est d'une échelle deux fois inférieure à l'axe horizontal. a) moyenne (des mesures à toutes les vitesses de cisaillement pour chaque échantillon) du module de viscosité excédentaire, $\overline{G''_E}$; b) moyenne du module élastique, $\overline{G'}$ (toute mesure faite à $\dot{\gamma}$ = 0,973 s^{-1} est exclue de la moyenne).

Mediterranean and North Sea data sets. In the corresponding parts of the curves where $\overline{G''_E}$ was negative (and where log(- $\overline{G''_E}$) was plotted against scaled rank), no straight line section appears with decreasing rank, the curves for both sea areas remaining rather concave. The highest negative value of $\overline{G''_E}$ recorded were rather similar, - 6.3 μPa (Mediterranean) and - 3.3 μPa (North Sea). The positive near-zero parts and the negative parts of the curves for the two data sets resemble each other in both value and slope, indicating similar means and SD_G. At high positive values, however, both value and slope are markedly different. This is interpreted as indicating similar means and SD_G for each of the two data sets for those parts of the data dominated by measurement artefacts, but very different values and variance for the parts dominated by environmental properties.

It is concluded that at values of $\overline{G''_E}$ high enough for the environmental component to be separated from measurement artefacts (~ 2 μPa), the North Sea samples possessed higher mean and SD_G in excess viscosity than the Mediterranean samples. Part of this extra variability may have derived from the sampling strategy, which targeted five hydrological layers in the North Sea, including the air-sea and the sea-sediment interfaces, while the Mediterranean study involved mainly mid-water layers. Although no biological measurements exist for our Mediterranean data set, further variability in the North Sea samples as well as their higher mean values may have resulted from higher abundance and patchiness in polymer content associated with the abundant and patchy distribution of phytoplankton.

DISCUSSION

Bulk-phase rheological properties of the samples

At $\dot{\gamma}$ = 0.0021 s^{-1}, the measured viscosity of the meso-oligotrophic Mediterranean seawater samples was 0.71 to 19 times that of the solution viscosity η_W, which is due to water and salts alone. The corresponding values for $\dot{\gamma}$ = 0.286 s^{-1} were 0.92 to 1.12.

At $\dot{\gamma}$ = 0.0021 s^{-1} the viscosity of samples taken from the North Sea, where patchy blooms of *Noctiluca scintillans* and *Phaeocystis* sp. were taking place was 0.99 to 127 times η_W. Viscosity at $\dot{\gamma}$ = 0.286 s^{-1} was 0.96 to 3.2, and at $\dot{\gamma}$ = 0.973 s^{-1} it was 0.98 to 1.21 times η_W.

That values of SD $[\eta_E(\dot{\gamma})]/\overline{\eta_E(\dot{\gamma})}$ or each cruise and shear rate (except at the lowest value of $\overline{\eta_E(\dot{\gamma})}$, where measure-

ment error is believed to have been dominant), varied from about 1 to about 3 indicates a very high rheological patchiness or "lumpiness". Despite the vigorous mixing associated with sampling, this lumpiness was present within the samples from which duplicate 0.5 to 1.0 cm^3 subsamples were measured. This suggests that centimetre-scale (or smaller) flocculation occurred in the samples during storage and transport (less than about one day). Flocculation is important in marine colloids (Morel and Gschwend, 1987), and cm-scale variation in fluorescence *in situ* may reflect similar variation in polymer concentration and viscosity (Carlson, 1991). The observation of exceptional thickening in some plankton blooms (*see* "Introduction"), the correlation between η_E and chlorophyll concentration in the present North Sea study (Jenkinson and Biddanda, in preparation), and the increased bulk-phase viscosity found in some surface slicks (Carlson, 1987) indicates that seawater thickening varies also at larger scales.

Carlson *et al.* (1987) suggested that artificially high values of viscosity might be produced in CS rheometry due to colloidal material being scavenged from the bulk phase on to the surfaces of the CS. That surface effects in the CS were found to increase frequently over time suggests that organics are scavenged by the air-seawater interface. Any scavenging on to either the air-liquid surface or the metal-liquid surface would take polymers out of the bulk phase, and would tend to reduce bulk-phase thickening. Adsorption on to the cleaned glass walls of the sampling bottles might have further reduced measured values of thickening.

Generally, in gels $P \geq 1$, but in polymers without cross-links, $P < 1$ and a Newtonian plateau in η ($P = 0$) occurs over a range of $\dot{\gamma}$ (Morris, 1984). The consistently high values of P found over two or more orders of magnitude in $\dot{\gamma}$ in the present study, thus suggest that the non-Newtonian behaviour was contributed largely by highly cross-linked gel. Material secreted into culture by green and red algae, was shown by its turbulent-drag reducing properties to consist of very complex, polymeric, aggregative gels (Ramus and Kenney, 1989; Ramus *et al.*, 1989). In contrast, the viscosity of a culture of *Amphidinium?* sp. over a range of $\dot{\gamma}$ from 0.017 to 129 s^{-1} showed a low-$\dot{\gamma}$ Newtonian plateau ($P \sim 0$), and a higher range of $\dot{\gamma}$ in which $P \sim 0.5$ (Jenkinson, 1986), indicating that thickening was due principally to overlapping polymer molecules (Morris, 1984; Barnes *et al.*, 1989). Similarly, in cultures of *Dunaliella marina* and of *Noctiluca scintillans* together with *D. marina* (Jenkinson, 1986), as well as in a culture of *Gyrodinium cf. aureolum* and in water filtered from a suspension of *N. scintillans* (Jenkinson, 1993), no low-$\dot{\gamma}$ plateaux occurred, values of P were lower than in the present work, and inflexions, including steps, occurred in the slope. This suggests that both cross-linking and overlapping of the polymers were responsible for the rheological properties to different relative extents at different shear rates.

A ratio around unity (0.22 to 11) is indicated for G'/G''_E in the bulk-phase polymeric material in the present study. Corresponding to their lower values of P, values obtained for G'/G''_E were also generally lower in phytoplankton suspensions, further suggesting a less cross-linked polymer structure. Values for G'/G''_E were: 0.4 in the mixed culture of *Noctiluca scintillans* and *Dunaliella marina* (calculated from data presented by Jenkinson, 1986); 0.2 to 0.9 in the culture of *Gyrodinium cf. aureolum*, mentioned above; 0.2 to 0.3 in water filtered from a suspension of *N. scintillans* (Jenkinson, 1993). Similarly Frew and Nelson (1992) found that the ratios of both (surface-film compression elastic modulus)/(film pressure) and carbon/nitrogen were higher in samples from an area relatively low in biological activity, suggesting that the film material had, in ageing, become more cross-linked.

Silicate and organic C are present in seawater in comparable amounts, ~ 0.2 and ~ 0.1 mM respectively, and both form polymeric complexes, although silicate begins to polymerise at concentrations ≥ 1.5 mM (Stumm and Morgan, 1981). Dissolved silicate strengthens some organic polymers by cross-linking and is surface active (Schwarz, 1973; Grant and Long, 1985; Jarvie, 1986; Zhang *et al.*, 1991). Silicate may thus enhance seawater rheological properties by adsorbing on to surfaces provided by colloidal organic polymers (Morel and Gschwend, 1987). The idea is somewhat supported by Hollibaugh *et al.*'s (1991) finding that "dissolved" silicate is occasionally retained by ultrafiltration.

Possible origin of surface-film shear forces

When shear forces in the surface film were measured in continuous rotation of the CS, the regular, and frequently approximately sinusoidal, oscillation of these forces with the same period as that of CS rotation indicates a large degree of spatial integrity in the surface film during rotation. Exactly how this integrity was maintained remains unknown, although interaction of two plaques, one adhering to the bob and the other to the wall of the cup, seems likely (Lavèn, personal communication).

Measurements made with both continuous rotation and sinusoidal oscillation, as well as with both the surface-phase bob and with the bulk-phase bobs, gave the following maximum shear strengths: 2 mN m^{-1} for *Skeletonema* culture; 0.17 for aged distilled water; 0.03 for 0.2-μm filtered seawater; 0.03 mN m^{-1} for unfiltered or filtered (0.5 mm) seawater samples. The relatively high value for the *Skeletonema* culture suggests that diatoms and their setae might have reinforced the material habitually in the surface film, a mechanism suggested by Wyatt *et al.* (1993) for the bulk phase. No previous data on shear properties appear to exist for the seawater surface film. For film pressure (*i. e.* compression strength), however, Van Vleet and Williams (1983) found values in sea-surface films of 1.5 to 15 mN m^{-1}, about two orders of magnitude higher than the maximum shear forces we measured in the surface film of seawater. Ting *et al.* (1984), working with surface films of octanoic acid, also found film pressure to be about two orders of magnitude higher than shear strength, so shear strength and film pressure in sea-surface films may each be produced by the same material. Barger and Means (1985), who also measured film pressures, concluded that surface films are composed of material similar to very large poly-

mers, occupying about 400 to 800 nm^2 per molecule. This material is highly oxidised, suggesting that it is largely polysaccharide. Lipids comprise ~ 2-5 % of surface film material, but film pressure-area graphs scaled to lipid content are relatively constant (Frew and Nelson, 1992), suggesting that lipid may contribute disproportionately to surface-film rheological properties. Silica particles adsorb at surfaces, where they increase considerably the elastic modulus of surface films (Zhang *et al.*, 1991). They also adsorb at the sea surface in amounts up to 3 mM (Szekielda *et al.*, 1972), where they may also toughen organic films.

Might organic matter contribute to the high-shear component of η_W?

To estimate the role of salinity in determining seawater viscosity, Miyake and Koizumi (1948) measured high-$\dot{\gamma}$ viscosity in increasingly diluted seawater. Assuming that they used pure water as dilutant, they diluted the non-conservative organic matter along with the conservative salt. Interference by surfactants or sticky material may furthermore be suspected from Miyake and Koizumi's observation that, "The most important source of error might be due to a delicate change in the condition of the inner wall of the capillary, but it was impossible to estimate its exact magnitude". Some organic matter might contribute to η_W. To separate η_W from η_E in future studies, it will be necessary to make high-$\dot{\gamma}$ measurements on waters of different original salinity.

That, in the present study, some values of η_E have been calculated as negative could reflect (in addition to experimental errors) a non-conservative polymeric component contributing to high-$\dot{\gamma}$ viscosity.

Importance of viscoelastic thickening to turbulence and mixing

A simple model was proposed by Jenkinson (1986) to predict the effect of homogeneous excess viscosity (as k and P) on Kolmogorovian (non-intermittent) turbulence. If the mean values of $\dot{\gamma}$-dependent $\overline{\eta_E(\dot{\gamma})}$ found on the five cruises of the present study (Tab. 2) are used in this model, the changes indicated in Figure 15 are obtained. The aim of this model is to provide only a quantitatively reasoned guess about modification of turbulence by polymeric thickening. Serious prediction must await better information about both rheological parameters and marine turbulence. Relevant rheological parameters for gels include: elastic modulus; yield stress; yield point; the same parameters for both shearing and extensional (also called elongational) flow; time dependence of all these parameters. The variation of all these parameters with length scale, together with lump shape, are also critical. Because turbulence is always intermittent and P is high, the excess viscosity increases intermittence by reducing deformation rates proportionately more when they are already low. For a given overall intensity of turbulence (rms $\dot{\gamma}$) when other things are equal, mixing parameters should *in addition* be negatively related both to G' and to the Trouton ratio (elongational viscosity/shear viscosity) (Barnes *et al.*, 1989). Furthermore, lumpiness (*i. e.* SD_G) in each of these parameters should contribute to increased intermittence and reduced mixing. Wyatt *et al.* (1993) have suggested how viscosity and structure may be contributed to bulk-phase seawater, otherwise than by polymers.

CONCLUSIONS

The viscosity of bulk seawater is composed of a Newtonian viscosity η_W, due to water and salt and independent of shear rate, on which is imposed an excess viscosity η_E related to shear rate by an inverse power law. Total viscosity,

$\eta = \eta_W + \eta_E$, where $\eta_E = k.\dot{\gamma}^{-P}$

Since P was found to exceed 1, the seawater possesses a yield stress, which is a shear stress ($\eta.\dot{\gamma}$) below which the sea water gels. Strongly covarying with η_E is a measurable elastic modulus G'. Both η_E and G' are distributed in a lumpy (rheologically heterogeneous) fashion, and are due

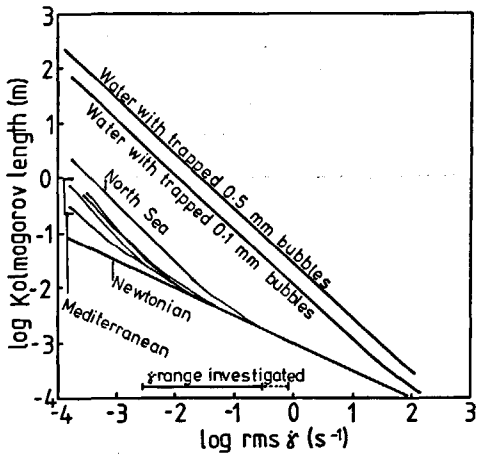

Figure 15

Effect of measured and observed thickening on the Kolmogorov length-scale, calculated from my previous model (Jenkinson, 1986). Actual turbulent length scale is around forty times that of the Kolmogorov scale (Jenkinson, 1986; Lazier and Mann, 1988; Yamazaki et al., *1991). The curves represent the arithmetic mean viscometric properties [relation of* $\eta(\dot{\gamma})$ *to* $\dot{\gamma}$*] for each Mediterranean and North Sea cruise. For comparison, curves for Newtonian (unthickened) water and for* Gyrodinium *cf.* aureolum*-bloom water observed to trap 0.1 to 0.5 mm diameter bubbles (assuming that P = 1) are also shown. Effects of elasticity, lumpiness, time dependence, elongational viscosity,* etc. *are not taken into account.*

L'effet des épaississements mesurés et observés sur l'échelle de longueur de Kolmogorov, estimé à partir de mon modèle antérieur (Jenkinson, 1986). La vraie échelle de longueur turbulente est environ quarante fois plus importante (Jenkinson, 1986 ; Lazier et Mann, 1988 ; Yamasaki *et al.*, 1991). Les courbes représentent les moyennes arithmétiques des propriétés viscométriques [relation entre $\eta(\dot{\gamma})$ et $\dot{\gamma}$] pour chaque sortie en Méditerranée et pour la croisière en Mer du Nord. Pour comparaison, les courbes correspondantes sont données pour l'eau newtonienne (non-épaissie), ainsi que pour l'eau dans une floraison de *Gyrodinium* cf. *aureolum*, où a été observée la rétention de bulles de diamètre compris entre 0,1 et 0,5 mm (il est supposé ici que P = 1). Les effets, entre autres, de l'élasticité, de la floculation en grumeaux, de la dépendance du temps et de la viscosité élongationelle ne sont pas pris en compte.

principally to organic polymers with a flocculent tendency, produced largely by phytoplankton. These polymers appear similar to, and exchange with, those responsible for viscosity and elasticity in the sea-surface film. A model of turbulent length scale in relation to η, predicts that turbulence is damped the most, in relative terms, both in zones already low in turbulence and in those of high biopolymer content. The high value of P and the lumpy distributions of both η_E and G' all make turbulence more intermittent. In much of the sea, flow and mixing, particularly at small scales ($\leq$ 100.Kolmogorov length), are under strong biological influence.

Acknowledgements

This work has been supported by: the University of Nice-Sophia Antipolis with an Associate Assistantship; the Alfred-Wegener-Institute with a Guest Research Fellowship; the clients of ACRO, who have recycled their funds within oceanography.

For hospitality, help in the laboratory and at sea, for sharing their data and equipment, for their ideas and for correcting mine, I particularly thank: E.R. Morris (Bedford, England); V. Smetacek, P. Abreu, B. Biddanda, S. Elken, K. Müller, M. Pamatmat, R. Plugge, U. Riebesell, F. Rieman, K. Schaumann, C. Turley, E. Wahl, C. Wiencke and the master and crew of the *Victor Hensen* (Bremerhaven); J. Lavèn (Eindhoven); M. Rinaudo and M. Milas (Grenoble); H. von Westernhagen (Hamburg); G. Uhlig (Helgoland); J. Aleman (Madrid); R. Vaissière (Monaco); G. Herndl (Vienna); T. Wyatt (Vigo); P. Nival, M. Corre, J. Delarue and G. Gorsky (Villefranche-sur-Mer). This paper has been meticulously corrected and improved by an anonymous referee.

REFERENCES

Barger W.R. and J.C. Means (1985). Clues to the structure of marine organic material from the study of physical properties of surface films, in: *Marine and Estuarine Geochemistry*, A.C. Sigler and A. Hattori, editors. Lewis, Chelsea, UK, 47-67.

Barnes H.A., J.F. Hutton and K. Walters (1989). *An Introduction to Rheology*. Elsevier, Amsterdam, 199 pp.

Benoit H. (1984). *Physics of Finely Divided Matter*, N. Boccara and M. Daoud, editors. Springer, Berlin, 2-15 (cited by Prost and Rondelez, 1991).

Carlson D.J. (1987). Viscosity of sea-surface slicks. *Nature*, **329**, 823-825.

Carlson D. (1991). *In situ* exploration of macromolecular and particulate materials in seawater, in: Marine Particles: Analysis and Characterization, D.C. Hurd and D.W. Spencer, editors. *Geophysical Monograph, Am. geophys. Union*, **63**, 195-198.

Carlson D.J., L.E. Morril and J.E. Brophy (1987). Techniques of fluorescence depolarization for measuring seawater viscosities. *Limnol. Oceanogr.*, **32**, 1377-1381.

Faurel X. (1989). Proposition de termes et définitions pour le Dictionnaire de Rhéologie. *Cah. Rhéol.*, **8**, 149-151.

Fogg G.E. (1991). The phytoplanktonic ways of life. *New Phytol.*, **118**, 191-232.

Frew N.M. and R.K. Nelson (1992). Scaling of marine microlayer film surface pressure-area isotherms using chemical attributes. *J. geophys. Res.*, **97**, C4, 5291-5300.

Frontier S. and D. Pichod-Viale (1991). *Écosystèmes : structure, fonctionnement, évolution*. Masson, Paris, 392 pp.

Grant W.D. and P.E. Long (1985). Environmental microbiology, in: *The Natural Environment and the Biogeochemical Cycles*, H.J.M. Bowden, T. Frevert, W.D. Grant, G. Kratz and P.E. Long, editors. Springer-Verlag, Berlin, 127-237.

Harvey G.W. and L.A. Burzell (1972). A simple microlayer method for small samples. *Limnol. Oceanogr.*, **17**, 156-157.

Hollibaugh J.T., R.W. Buddmeier and S.V. Smith (1991). Contribution of colloidal and high molecular weight dissolved material to alkalinity and nutrient concentrations in shallow marine and estuarine systems. *Mar. Chem.*, **34**, 1-27.

Hutchinson G.E. (1967). *A Treatise on Limnology. Vol. 2*. John Wiley, New York, 1115 pp.

Jarvie A.W.P. (1986). Environmental aspects of organosilicon and use, in: *Organometallic Compounds in the Environment*, P.J. Craig, editor. Longman Group, Harlow, England, 229-253.

Jenkinson I.R. (1986). Oceanographic implications of non-newtonian properties found in phytoplankton cultures. *Nature*, **323**, 435-437.

Jenkinson I.R. (1989). Increases in viscosity may kill fish in some blooms, in: *Red Tides*, T. Okaichi, D.M. Anderson and T. Nemoto, editors. Elsevier, New York, 435-438.

Jenkinson I.R. (1990). Rheological structure in bulk seawater, in: *Third European Rheology Conference*, D.R. Oliver, editor. Elsevier, London, 247-251.

Jenkinson I.R. (1993). Viscosity and elasticity of *Gyrodinium* cf. *aureolum* and *Noctiluca scintillans* exudates in relation to mortality of fish and damping of turbulence, in: *Toxic Phytoplankton Blooms in the Sea*, T.J. Smayda and Y. Shimizu, editors. Elsevier, Amsterdam, 757-762.

Jenkinson I.R. and T. Wyatt (1992). Selection and control of Deborah numbers in plankton ecology. *J. Plankt. Res.*, **14**, 1697-1721.

Jenkinson I.R., B.A. Biddanda, C.M. Turley, P.C. Abreu, U. Riebesell and V.S. Smetacek (1991). Rheological properties of marine organic aggregates: importance for vertical flux, turbulence and microzones. *Proceedings of the International Colloquium on the environment of epicontinental seas, Lille, France, 20-22 March 1990, Oceanologica Acta*, **Vol. sp. No. 11**, 101-107.

Kolmogorov A.N. (1941 *a*). The local structure of turbulence in incompressible viscous fluid for very large Reynolds numbers. *C.r. Acad. Sci. USSR*, **30**, 310 (cited by Woods and Wiley, 1972).

Kolmogorov A.N. (1941 *b*). On degeneration of isotropic turbulence in an incompressible viscous liquid. *C.r. Acad. Sci. USSR*, **31**, 538 (cited by Woods and Wiley, 1972).

Krümmel O. (1907). *Handbuch der Ozeanographie. Bd. I*. J. Engelhorn, Stuttgart, 526 pp.

Lazier J.R. and K.H. Mann (1988). Turbulence and diffusive layers around small organisms. *Deep-Sea Res.*, **36**, 1721-1733.

Margalef R. (1957). Nuevos aspectos del problema de la suspensión en los organismos planctónicos. *Invest. pesq.*, **7**, 105-116.

Margalef R. (1978). Life-forms of phytoplankton as survival alternatives in an unstable environment. *Oceanologica Acta*, **1**, 4, 493-509.

Miyake Y. and M. Koizumi (1948). The measurement of the viscosity coefficient of sea water. *J. mar. Res.*, **7**, 63-66.

Morel F.M.M. and P.M. Gschwend (1987). The role of colloids in the partitioning of solutes in natural waters, in: *Aquatic Surface Chemistry*, W. Stumm, editor. John Wiley, New York, 405-422.

Morris E.R. (1984). Rheology of Hydrocolloids, in: *Gums and Stabilisers for the Food Industry. 2: Applications of Hydrocolloids*, G.O. Phillips, D.J. Wedlock and P.A. Williams, editors. Pergamon, Oxford, UK, 57-78.

Prost J. and F. Rondelez (1991). Structures in colloidal physical chemistry. *Nature, suppl.*, **350**, 11-23.

Ramus J. and B.E. Kenney (1989). Shear degradation as a probe of microalgal exopolymer structure and rheological properties. *Biotechnol. Bioengng*, **34**, 1203-1208.

Ramus J., B.E. Kenney and E.J. Shaughnessey (1989). Drag reducing properties of microalgal exopolymers. *Biotechnol. Bioengng*, **33**, 550-557.

Saasen A. and O. Hassager (1991). Gravity waves and Rayleigh-Taylor instability on a Jeffrey-fluid. *Rheol. Acta*, **30**, 301-306.

Schwarz K. (1973). Bound form of silicon in glycosaminoglycans and polyurones (polysaccharide matrix/connective tissue). *Proc. natn Acad. Sci. U.S.A.*, **70**, 1608-1612.

Sournia A. (1982). Form and function in marine phytoplankton. *Biol. Rev.*, **57**, 347-394.

Stachowitsch M., N. Fanuko and M. Richter (1990). Mucus aggregates in the Adriatic Sea: an overview of stages and occurrences. *Pubbl. Staz. zool. Napoli: Mar. Ecol.*, **11**, 327-350.

Stumm W. and J.J. Morgan (1981). *Aquatic Chemistry: an Introduction Emphasizing Chemical Equilibria in Natural Waters.* John Wiley, New York, 780 pp.

Sugimura Y. and Y. Suzuki (1988). A high temperature catalytic oxidation method for non-volatile dissolved organic carbon in seawater by direct injection of liquid sample. *Mar. Chem.*, **24**, 105-131.

Szekielda K.-H., S.L. Kupferman, V. Klemas and D.F. Polis (1972). Element enrichment in organic films and foams associated with aquatic frontal systems. *J. geophys. Res.*, **77**, 5278-5282.

Ting L., D.T. Wasan, K. Miyano and S.-Q. Xu (1984). Longitudinal surface waves for the study of dynamic properties of surfactant systems. II: Air-solution interface. *J. Colloid Interface Sci.*, **102**, 248-259.

Van Vleet E.S. and P.M. Williams (1983). Surface potential and film pressure measurements in seawater systems. *Limnol. Oceanogr.*, **28**, 401-414.

Williams P.R. and D.J.A. Williams (1989). Rheometry for concentrated cohesive suspensions. *J. coast. Res., Spec. Issue*, **No. 5**, 151-164.

Woods J.D. and R.L. Wiley (1972). Billow turbulence and ocean microstructure. *Deep-Sea Res.*,**19**, 87-121.

Wyatt T., F.G. Figueiras and F. Rios (1993). The impact of phytoplankton suspensions on seawater viscosity, in: *Toxic Phytoplankton Blooms in the Sea*, T.J. Smayda and Y. Shimizu, editors. Elsevier, Amsterdam, 849-853.

Yamazaki H., T.R. Osborn and K.D. Squires (1991). Direct numerical simulation of planktonic contact rates in turbulent flow. *J. Plankt. Res.*, **13**, 629-643.

Zhang K.-w., F.-q. Tang and L. Jiang (1991). Film-forming ability of submicrometer silica particles. *Langmuir*, **7**, 1293-1295.